Deep–Sea Research II xxx (xxxx) xxx

Contents lists available at ScienceDirect

Deep-Sea Research Part II

journal homepage: http://www.elsevier.com/locate/dsr2

Hydrography of the Eastern Mediterranean basin derived from argo floats profile data

Dimitris Kassis, PhD, Post-Doc Researcher *, Gerasimos Korres, PhD, Research Director

Institute of Oceanography, Hellenic Centre for Marine Research, PO Box 712 Anavyssos, Attica, GR-190 13, Greece

ARTICLE INFO

Keywords:
Heat content
Salt content
Water formation
Water masses
Profiling floats

ABSTRACT

As the Eastern Mediterranean integrates different sub-basins with important hydrological features, during recent decades it has often become a target of study by the oceanographic community. The recent expansion of observational tools and methods in the marginal seas has allowed more enhanced studies of the oceanographic processes that dominate such areas. In this work, temperature and salinity profile data collected by Argo floats in the Eastern Mediterranean are analysed for the period 2004–2017. The spatio-temporal variability of the basin's physical properties, together with the depicted changes in the different sub-basins, is investigated in an attempt to construct the latest hydrographic picture of the region. The findings describe the dominant water masses and reveal a general positive trend in the basin's thermohaline properties. The inter-annual variability of the stored heat and salt, and their distribution in the water column, reveals strong climatic signals that are dominated by previously reported alternations of the general circulation and convection events in the area. The latter are correlated with the surface temperature and salinity fields and are traced within the area's different sub-basins. In the early period (2004–2010), data from Levantine and Ionian depict inter-annual variability of the upper layers salinity field that is correlated with previously reported alternations of the Levantine's circulation, and intermediate water production in the Ionian. During the latest period (2012–2017), when the data coverage is denser and more representative for the wider area of the Eastern Mediterranean, the Adriatic sub-basin presents intense dense water production activity while the Aegean Sea undergoes a relaxation period with significant variability at intermediate layers due to water mass exchanges.

1. Introduction

The Mediterranean Sea is a semi-enclosed wide marginal basin at mid-latitudes separated by the Sicily Straits into two parts: the Western and the Eastern Mediterranean Sea. For the last 50 years, the area's hydrography has been under study from a large section of the oceanographic community. Several earlier studies (until 1990) have produced synthetic descriptions of the area's main hydrographic features that include the dominant water masses dynamics, the general circulation, and the climatological analyses (Guibout, 1987; Malanotte-Rizzoli and Hecht, 1988; Millot, 1987; Ovchinnikov, 1976). With regards to the Eastern Mediterranean, scientific questions such as Dense Water Formation (DWF) processes, circulation, and other fundamental oceanographic procedures, were further investigated, during the late 1980's, under the POEM (Physical Oceanography of the Eastern Mediterranean) project (Malanotte-Rizzoli and Robinson, 1988; Robinson et al., 1992; Roether and Schlitzer, 1991). Through these studies, it was shown that the circulation of the Eastern Mediterranean presents complex patterns that evolve in several different spatio-temporal scales. Furthermore, the area's main sub-basins (Levantine Sea, Aegean Sea, Ionian Sea, and Adriatic Sea), dynamically interact with each other, and play a very important role on the general hydrology of the basin. The dominant water masses that co-exist in the basin's water column, from the surface down to its deep layers are firstly the Levantine Surface Water (LSW) which has increased salinity and is produced in the Levantine basin especially during the summer period due to the surface warming and the excess of the evaporation in the area (Lascaratos et al., 1993). Secondly, the low-salinity Atlantic Water (AW) in the sub-surface zone which enters from the west into the Eastern Mediterranean via the Sicily Straits and moves further eastward forming the Atlantic Ionian Stream (AIS). Thirdly, the Levantine Intermediate Water (LIW) which is also produced in the Levantine during winter convection mainly over its central and northwestern parts (Lascaratos et al., 1993). After its formation, the LIW propagates from the east to the west into the Libyan, Aegean, Ionian, and

* Corresponding author.
E-mail addresses: dkassis@hcmr.gr (D. Kassis), gkorres@hcmr.gr (G. Korres).

https://doi.org/10.1016/j.dsr2.2019.104712
Received 18 December 2018; Received in revised form 10 December 2019; Accepted 14 December 2019
Available online 18 December 2019

Adriatic Seas with a characteristic high salinity signal at intermediate depths reaching the Western Mediterranean basin through complex and variable pathways (Wu and Haines, 1996). Finally, the remaining dominant water mass is defined as the Eastern Mediterranean Deep Water (EMDW), that fills the deep layers of the basin. The EMDW is formed mainly in the Ionian basin due to the mixing of deep LIW and denser water masses that originate from DWF events. Such events occur in the Adriatic where, during the winter period, the combination of cold northern winds and the presence of Levantine waters creates large buoyancy losses that lead to Adriatic Deep Water (AdDW) formation (Mantziafou and Lascaratos, 2008). The AdDW exits the Adriatic basin through the Otranto Strait into the deep horizons of the Ionian Sea and mixes with the pre-existing water masses to form EMDW. However, the Aegean Sea has also been identified as another source of deep-water formation, the Cretan Deep Water (CDW) that contributes to the production of EMDW with slightly different thermohaline characteristics. This process was closely investigated in the early 1990's when an important feature was revealed in the Eastern Mediterranean; the observation of an intense outflow of dense Aegean water via the Cretan Arc Straits. The Aegean Sea became the new source of deep water for the Eastern Mediterranean, a role that had only been assigned to Adriatic Sea until then. This dramatic transition is known as the Eastern Mediterranean Transient (EMT) (Klein et al., 1999; Lascaratos et al., 1999; Malanotte-Rizzoli et al., 1999; Roether et al., 1996; Theocharis et al., 1993). During the EMT, large amounts of the newly produced, warm (>14 °C), and saline (>39.1) CDW, spread out the Aegean through the Cretan Arc Straits lifting the pre-existing and less dense EMDW of the Ionian and Levantine basin by approximately 500 m (Roether et al., 2007). EMT was originally attributed to both regional meteorological anomalies (cold winters, reduced precipitation), and long-term salinity changes in the wider area related to climatic variability and anthropogenic activities (Lascaratos et al., 1999; Roether et al., 2007; Skliris, 2014; Theocharis et al., 1999; Tsimplis and Josey, 2001). Later studies have proposed several mechanisms and processes that associate EMT with a re-occurring transition of the basin's general circulation patterns, and the antagonistic roles of Adriatic and Aegean sub-basins towards deep water formation events and dense water outflow (Bergamasco and Malanotte-Rizzoli, 2010; Borzelli et al., 2009; Gačić et al., 2014, 2010; Theocharis et al., 2014).

In enclosed seas like the Mediterranean, the hydrological cycle is especially sensitive to climatic variability. Such variability triggers both severe meteorological conditions and hydrological transitions that create feedback mechanisms at different time scales. Hence, variability of the heat transfer rate, alternation of the general circulation patterns, cold winter periods, changes in the fluxes of evaporation over precipitation ($E - P$), and in rivers runoffs (R), can lead to strong thermal, and haline, density fluxes, and alternate the heat and salt content. During the second half of the last century the heat and water budgets across the Mediterranean sea surface have been estimated to be approximately 1.74 W m^{-2}, corresponding to an increase of 0.4 °C for the sea-surface temperature and an increase of 0.1 m (or 11%) in the freshwater deficit (partly associated to both climatic change and human activities) (Béthoux et al., 1998). The estimated temperature changes in different layers and locations between 1940 and 1995 have been imprinted in the increase of the heat content of the Mediterranean Sea by a mean value of 0.65 W m^{-2} (0.53 and 0.70 W m^{-2} in the western and eastern basin, respectively) (Béthoux et al., 1998). In more recent periods (1976–2000), the mean annual temperature rise is amongst the highest throughout the global oceans, whilst a decrease in the annual precipitation rates, with different seasonal trends, have been also reported (Drobinski et al., 2014). Estimations of the water budget in the Mediterranean Sea during the same period have indicated a water loss that ranges from 500 to 700 mm yr^{-1} due to the excess of $E - P$ (Mariotti et al., 2002). In other studies, the net flux of $E - P$ is estimated as being slightly above 0.70 m yr^{-1} whilst, for the eastern part the mean $E - P$ values are higher (0.81–0.85 m yr^{-1}) (Josey, 2003). Specifically for the Eastern Mediterranean, the reported increasing trends (0.05 °C yr^{-1}) of the Sea Surface Temperature (SST) derived from satellite observations from 1985 to 2006 (Nykjaer, 2009) is a major factor of increased expected heat and salt fluxes from the surface to the deeper layers, mainly via vertical mixing and convection events. Such is the LIW formation process during the summer period when intense warming leads to intensive evaporation and consequently increase of the surface salinity (Lascaratos et al., 1993). This, in turn, creates pre-conditioning for DWF, and vertical convection occurs during February and March when the surface cooling becomes intense. The newly formed LIW mixes, with the underlying AW and the pre-existing LIW, ventilate the depth zone 200–400 m, with saltier and warmer water masses (Özsoy et al., 1989). Recent observations on the Mediterranean Sea have suggested an enhanced freshwater deficit due to the further decrease of the precipitation and increase in the evaporation rates (Mariotti, 2010). Other studies have highlighted the impacts of the river runoff and freshwater input on the salt content in the Eastern Mediterranean. Such examples are the drastic changes in the Nile runoff after the construction of the Aswan dam (Skliris et al., 2007), and the alternations of the Black Sea Water (BSW) inflow into the Aegean Sea from the Dardanelles straits (Zervakis and Georgopoulos, 2002), which is considered as a possible driving mechanism of the EMT. In the EMT case, during winters of 1991, 1992 and, 1993, the mean air temperature over the Aegean Sea was recorded as being 2 °C lower than average whilst, for the period 1989–1993 the precipitation rate was lower (approximately 35 cm yr^{-1}) (Theocharis et al., 1999). The contribution of the atmospheric forcing was a major factor in the EMT case as, during that period, it was the anomalous northerly airflow of over the Aegean Sea that created strong latent heat losses which in turn resulted in the observed strongly positive density flux anomaly (Josey, 2003). In more recent studies, the Aegean Sea has been again reported to be pre-conditioned for DWF (Kassis et al., 2015; Schroeder et al., 2013; Velaoras et al., 2014) indicating that the Eastern Mediterranean is again entering into an EMT-like event, albeit less intense (Cardin et al., 2015; Velaoras et al., 2015). In Velaoras et al. (2017) such events are explained in the north Aegean as being due to the exceptionally cold winter of 2016–2017 that resulted in heat loss comparable to the EMT period (1992–1993). In general, recent analyses of Eastern Mediterranean field data have shown positive temperature and salinity trends both in upper and intermediate layers (Kress et al., 2014; Schroeder et al., 2017). The fact that such trends are stronger than those observed globally (Schroeder et al., 2017), underlines the role of the Eastern Mediterranean's hydrography as an ideal natural laboratory for investigating climatic changes and pressures.

In this work, the recent evolution of the Eastern Mediterranean thermohaline properties are investigated through the analysis of the latest temperature and salinity (T-S) Argo profiles. Inter-annual changes and trends of the water column physical properties are investigated throughout the 14-years examined period (2004–2017). The variability of the stored heat and salt, along with the signals of the dominant water masses are presented with a focus on the area's main sub-regions in an attempt to describe their hydrography and interaction. We investigate their spatio-temporal variability on a yearly and inter-annual basis as derived from field measurements to reconstruct the latest hydrographic picture of the wider basin, reveal its response to climatic signals, and highlight the importance of the profile datasets that the Mediterranean Argo network has provided.

The paper is organised as follows. The "Datasets and data processing methods" section describes the Argo profiles dataset, the floats general configuration and technical characteristics, and the methods used for the data analysis. The "Results" section presents the outputs of the data analysis and an inter-comparison in regional, annual, and at an overall averaged scale. In the "Discussion" section the main results are further discussed in conjunction with existing studies. Finally, in the "Conclusions" section, the main outcomes are summarised.

2. Datasets & data processing methods

The introduction of free-drifting profilers (Argo floats) initiated a new era for the oceanographic monitoring of the global oceans. During the last 15 years, the autonomous free-drifting profilers are systematically used also in marginal seas like in the Eastern Mediterranean basin. The latter has been significantly enriched with Argo floats with increased spatial coverage especially after 2010. Such evolution is the outcome of the combined activities of Euro-Argo Research Infrastructure and the National Argo initiatives. The dataset used in this study consists of all available Argo *T-S* profiles for the period 2004–2017 within the rectangular-shaped area from 12° E to 41° E and 30° N to 46° N, after removing Argo profiles referring to the Black Sea (27.5°–41° E and 40.8°–46° N), and the Ligurian Sea (13°–16.1° E and 38°–42° N). In total 32798 profile data were flagged as 'good' by the Argo data quality control team of the Coriolis Data Assembly Centre (www.coriolis.eu.org/Observing-the-Ocean/ARGO). All the Argo profilers are equipped with the SBE 41/41CP pumped MicroCATs (www.seabird.com/sbe-41-argo-ctd/product-details?id=54627907875), with accuracies of 0.002 °C for *T,* 0.002 psu for *S* and 2.4 dbars for pressure (*P*). Nevertheless, for operating floats, the salinity accuracy is estimated to 0.01 psu (Riser et al., 2016; Wong et al., 2003). The majority of the floats in the Mediterranean are configured to perform profiles down to 1000 m among five-day drifting cycles at 350 m depth according to the MedArgo specifications (Poulain et al., 2007). However, there are floats in the area configured to drift at a 1000 m depth and descend to 2000 m in 10-day cycles according to International Argo specifications. The percentage of these floats over the total ranges approximately from 32% during the first years of study, to 26% during the years 2012–2017. Before the data analysis, and in order to exclude erroneous data, an assessment on the profile dataset was performed following the recommendations of Argo delayed mode quality control teams (i.e., additional statistical checks and visual inspection). In general, the majority of uncertainties induced in Argo measurements are due to pressure sensor drift (Barker et al., 2011), and a systematic effort has been given during the last decade to detect and remove such errors. Uncertainties are also traced in the salinity measurements due to drift of the conductivity sensors, however for temperature data, no significant drift problems have been reported (Levitus et al., 2012). For both pressure and salinity drifts, the Global Data Archive Centers have provided corrected profiles for a large number of floats. The remaining uncorrected profiles are flagged as "bad data" and have not been used in this study. For specific floats, only the first 150 profiles were used for further analysis since, according to the recommendation from Argo International Delayed Mode Quality control experts, a salinity drift has been depicted after 2 years of their operation. Data assessment of the remaining profiles was performed via a two-step approach. The first step included the following tests: a) the profile location was checked; b) the pressure monotony was checked and the accordance of the maximum pressure with the profile's location bathymetry; c) values outside climatological boundaries were excluded (12–31 °C and 35–40 psu for temperature and salinity respectively), and d) shallow profiles (<100 dbar), or profiles with few data, were excluded. The remaining profiles were vertically interpolated by using the piecewise cubic interpolation method to respect the data monotonicity and the local minima and maxima (Kassis et al., 2015). Since this study focuses on the actual field data interpretation, further spatio-temporal interpolation, statistical fitting, and grid production was avoided. This, however, preserved the profile distribution heterogeneity in space and time as shown in Fig. 1 and Table 1. The interpolation was applied from the depth level of 5 m down to 1500 m (the

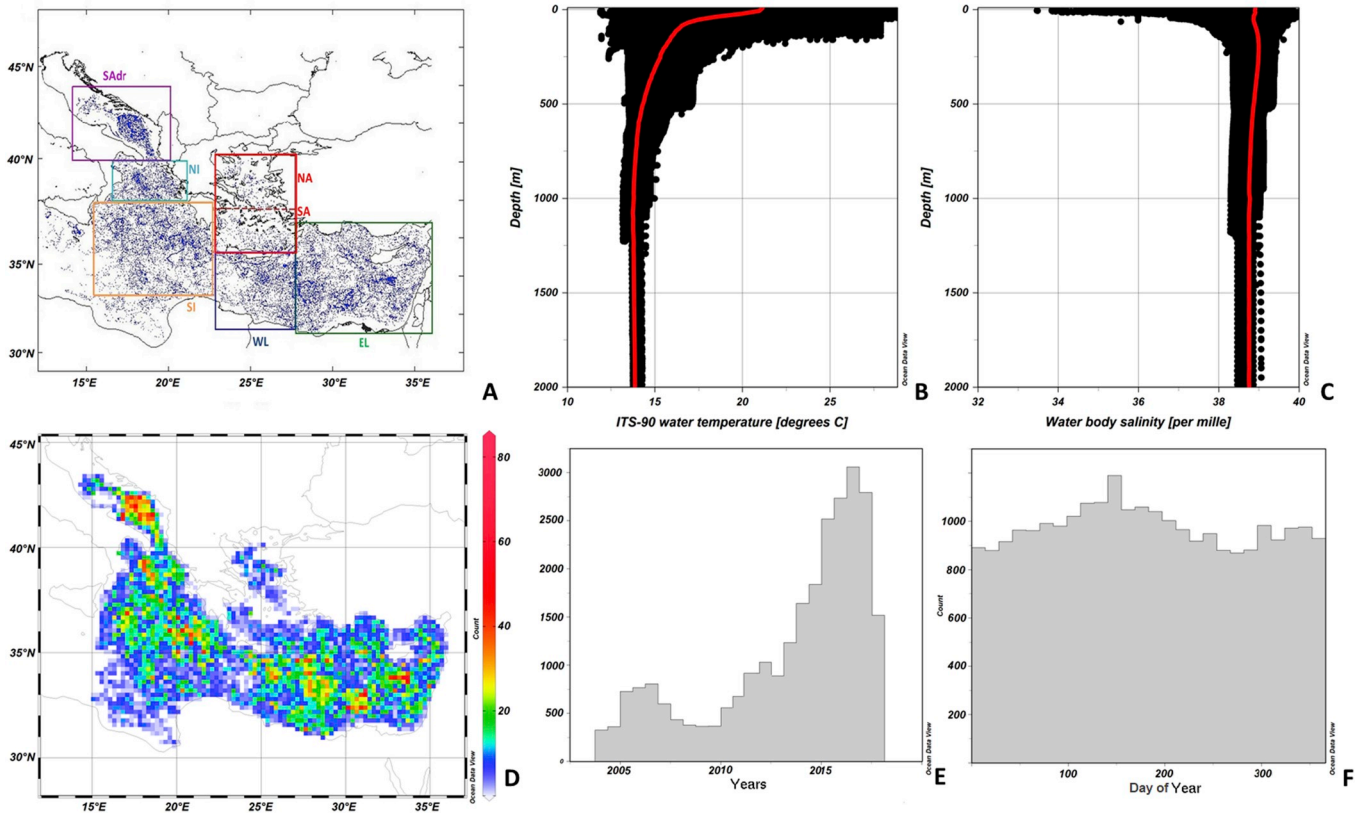

Fig. 1. A: Argo profiles mapped for the period 2004–2017. The sub-regions selected for the spatial analysis are presented: South-Adriatic (SAdr), North-Ionian (NI), South Ionian (SI), North and South Aegean (NA & SA), Western Levantine (WL) and, Eastern Levantine (EL). B: Temperature records from Argo profiles for the period 2004–2017 (red line indicates the mean). C: Salinity records from Argo profiles for the period 2004–2017 (red line indicates the mean). D: Spatial coverage of Argo profiles for the period 2004–2017. D: Temporal distribution of Argo profiles for the period 2004–2017. E: Distribution of profiles per day of year for the period 2004–2017. (For interpretation of the references to colour in this figure legend, the reader is referred to the Web version of this article.)

Table 1
Number of valid profiles per region, year and season.

Year	Eastern Levantine		Western Levantine		Aegean		South Ionian		North Ionian		South Adriatic		Eastern Mediterranean	
Season	Cold	Warm	Cold	Warm	Cold	Warm	Cold	Warm	Cold	Warm	Cold	Warm	Cold	Warm
2004	275	246	51	4	N/A	N/A	48	37	N/A	N/A	N/A	N/A	383	287
2005	216	250	78	35	10	3	110	96	18	34	N/A	N/A	480	484
2006	236	199	183	195	N/A	N/A	91	60	16	4	N/A	N/A	574	568
2007	166	147	126	132	N/A	N/A	79	69	N/A	N/A	N/A	N/A	399	380
2008	137	170	51	38	N/A	N/A	77	92	6	N/A	N/A	N/A	291	312
2009	146	104	11	3	N/A	N/A	92	68	18	11	N/A	N/A	311	238
2010	151	124	42	28	12	26	60	62	10	N/A	40	36	350	300
2011	45	40	14	13	33	15	156	199	14	37	37	36	322	390
2012	118	157	63	86	23	1	188	255	67	109	47	67	587	721
2013	278	248	29	71	14	1	370	404	60	92	130	254	1035	1125
2014	431	376	147	194	67	21	420	390	235	208	319	308	1645	1526
2015	559	719	295	604	110	161	582	698	180	131	217	196	2035	2600
2016	880	1011	495	383	69	60	794	863	114	125	191	217	2725	2811
2017	625	406	395	220	115	203	526	688	158	167	142	157	2034	1927
total	**4263**	**4197**	**1980**	**2006**	**453**	**491**	**3593**	**3981**	**896**	**918**	**1123**	**1271**	**13171**	**13669**

values above 5 m depth were excluded since the salinity values may introduce errors due to the floats' pump inactivation near the sea surface). After the interpolation, the second step of the assessment which ensured a) the rate of change of both *T* and *S* with depth should not exceed pre-defined thresholds (0.5 °C m^{-1} for temperature and 0.1 psu m^{-1} for salinity, below 20 m depth), and b) data-points that did not include all three *T*, *S* and *P* values were excluded from the analysis. The final homogenised dataset was spatiotemporally classified per year and per sub-region. The area was divided in 6 sub-regions taking into account spatio-temporal criteria such as the topography for semi-enclosed basins (ex. Aegean, Adriatic), the distinct physical characteristics/water masses exchanges between the different sub-regions (ex. North Ionian with Adriatic, South Ionian with Western Mediterranean, Aegean and Western Levantine, Western Levantine with Aegean, etc.), and finally, the overall profile coverage and the representation of each area. The spatial division (Fig. 1 A) was performed as follows: i) Aegean, covering the area from 22.84° E to 27.7° E and 35.26° N to 41° N; ii) South Ionian, covering the area from 15.34° E to 22.84° E and 33° N to 37.8° N; iii) North Ionian, covering the area from 16° E to 21.2° E and 37.8° N to 40°N; iv) Western Levantine, covering the area from 22.84° E to 28° E and 31.5° N to 35.1°N; v) Eastern Levantine, covering the area from 28° E to 36° E and 31.45° N to 36.8°N; vi) Central-south Adriatic, covering the area from 14.5° E to 20° E and 40° N to 44°N. A further classification regarding the seasonal distribution of the profiles per sub-region was also performed. Two seasonal periods are chosen to represent the "warm" semester (May–October), when intense thermocline is found in the upper layers, and the "cold" semester (November–April), when the stratification of the same layers is weakest. The fact that, in general, the profile data seem to be homogenously distributed seasonally (apart from few exceptions) (Fig. 1, Table 1), reduces the possibility of inherent biases during the yearly averaging process (Fig. 1A and B, C). Nevertheless, to minimise seasonal temperature signals, yearly temperature averaging in the upper layers has been generally avoided. Thus, the temperature statistical analysis is performed for depths below 100 m to avoid strongly unbalanced estimates derived from the variable seasonal profile distribution amongst the sub-basins, especially during the first 10-year period. Regarding the spatial distribution of the profiles, the statistical analysis depicted increased inter-annual coverage of the central Levantine and Ionian areas and the southern Adriatic. On the contrary, the southern part of Ionian, the northern part of Levantine, and the Aegean Sea are the most under-sampled areas (Fig. 1 D). The inter-annual distribution of the profiles of the whole domain presents a decrease after 2006 and rises again after 2010 reaching a peak of more 5500 profiles during 2016 (Fig. 1 E, Table 1). The seasonal and daily profile distributions are generally homogenous, with a slightly increased number of profiles during the late spring and early summer periods (Fig. 1 F). The grouped profiles from each area and year were visually inspected, and dubious data were also extracted from further analysis, thus the final dataset consisted of 26840 valid profiles; approximately 5% of the values were removed due to the aforementioned data quality control procedure. Parameters such as potential temperature, potential density - σ_θ, Mixed layer Depth (MLD), Brunt-Väisälä Frequency (BVF), Ocean Heat and Salt Content (OHC, OSC) were also calculated for each profile whilst, a statistical analysis was also performed for the estimation of the minima – maxima, average values and Standard Deviation (STD) per area, year and depth level. For the estimation of OHC and OSC for each profile the following equations (Eq. (1) and (2)) were used:

$$OHC = \rho_z C_p \int_{z2}^{z1} T_z dz \quad (1)$$

$$OSC = \int_{z2}^{z1} S_z dz \quad (2)$$

where ρ_z is the profile of the seawater density, C_p is the profile of the specific heat of seawater, z_1 is the upper (10 m) depth level, z_2 is the lower (1000 m) depth level, and T_z, S_z are the vertically interpolated temperature and salinity profiles. The yearly OHC and OSC per profile and region and their STDs are estimated by averaging the relevant individual OHC and OSC. Thus, the properties presented hereafter represent the yearly average OHC and OSC per profile, and not the total OHC and OSC of an area. The latter would require the construction of 3D-gridded estimated fields and their corresponding errors along with the construction of monthly fields as previously done for the global ocean estimates (Gaillard et al., 2015; Von Schuckmann et al., 2009). For the Eastern Mediterranean case which is poorly observed, an analysis based on *in-situ* observations alone it is still difficult to result in true total OHC and OSC quantities (Gaillard et al., 2015). For the estimation of MLD, the de Boyer Montégut et al. (2004) method was used with joint threshold criteria of *T* and σ_θ of 0.2 °C and 0.03 kg m^{-3} respectively, and 10 m surface reference level so as to avoid the diurnal heating of the surface layers as described in Kassis et al. (2016). The MLD seasonal variability in the Mediterranean is characterised by a deepening which typically starts in late November and continues until early April when an abrupt stratification occurs due to seasonal warming (D'Ortenzio et al., 2005), thus, selected periods were chosen accordingly to identify areas of deep MLDs.

3. Results

Both temperature and salinity data in the Eastern Mediterranean depict inter-annual variability at different depth layers. Due to the scarcity of data in the Aegean and Adriatic basins up until 2010, profile data from the Levantine and south Ionian areas that present inter-annual coverage, are analysed separately, and the yearly averaged profiles are

used for the presentation of the *T-S* temporal evolution throughout the whole study period. In the surface and sub-surface zones, temperature ranges from 13.2 to 30.25 °C. The maximum yearly averages in the warm periods of years 2008 and 2012, whilst the winter of 2004 presents the minimum yearly average. Salinity ranges from 37.09 to 39.68 psu and reaches the maximum average within the first 10 m in 2008 (39.13 psu), and a minimum average in 2010 (38.48 psu). In the 20–60 m sub-surface zone, the low salinity signal associated with the presence of AW, is intensely variable. The strongest signal is recorded in 2011 as being well below 38.5 psu, and in the following years (2012–2014), the signal is still present with values below 38.87 psu (Fig. 3). In the intermediate zone (200–600 m), the relatively cold-water masses that dominate during 2004–2006 are gradually replaced with warmer masses. After reaching a peak temperature during 2010 (15.58 °C on average at 300 m), in the following years, the temperature in these layers is reduced (Fig. 2), albeit stable, at approximately 0.1 °C degree higher than the previous period. Such variability is also evident for the intermediate zone in the salinity data that depicts a gradual increase after 2006, reaching a peak in 2010 (39.11 psu yearly average at 260 m), which decreases during the following years. Noteworthily, the LIW core that dominates in these depth layers is present throughout the study period in the depth zone between 180 and 350 m. In general, the anomalies in the *T-S* field that are depicted in the period 2008–2011, reflect the intense warming and salinization of the intermediate layers that had already started in 2006, and the sharp decrease of the sub-surface salinity in 2011. However, especially for the intermediate layers, the large standard deviation depicted during that period (Figs. 2 B, 3 B) highlights the fact that these anomalies do not reflect changes in the whole area of Levantine and Ionian, but rather localised processes that took place in certain sub-domains. Thus, the large *T-S* variation presented between 2009 and 2010 at intermediate depths cannot be considered as representative of large-scale changes to water properties. For the deep layers (1000–1500 m), the profile data availability is approximately 13% of the total profile dataset. In these data, the temperature spans from 13.55 to 13.75 °C, with the maximum average being observed during 2005. The same is presented in the deep layer salinity data; however, the few available deep profiles during that year do not provide enough certainty regarding these maxima. Nevertheless, it is of interest to note that general positive trends in temperature and salinity are recorded after 2013 in both intermediate and deep layers.

The data analysis on the different sub-regions reveals the contribution of each area towards the *T-S* long-term distribution in the Eastern

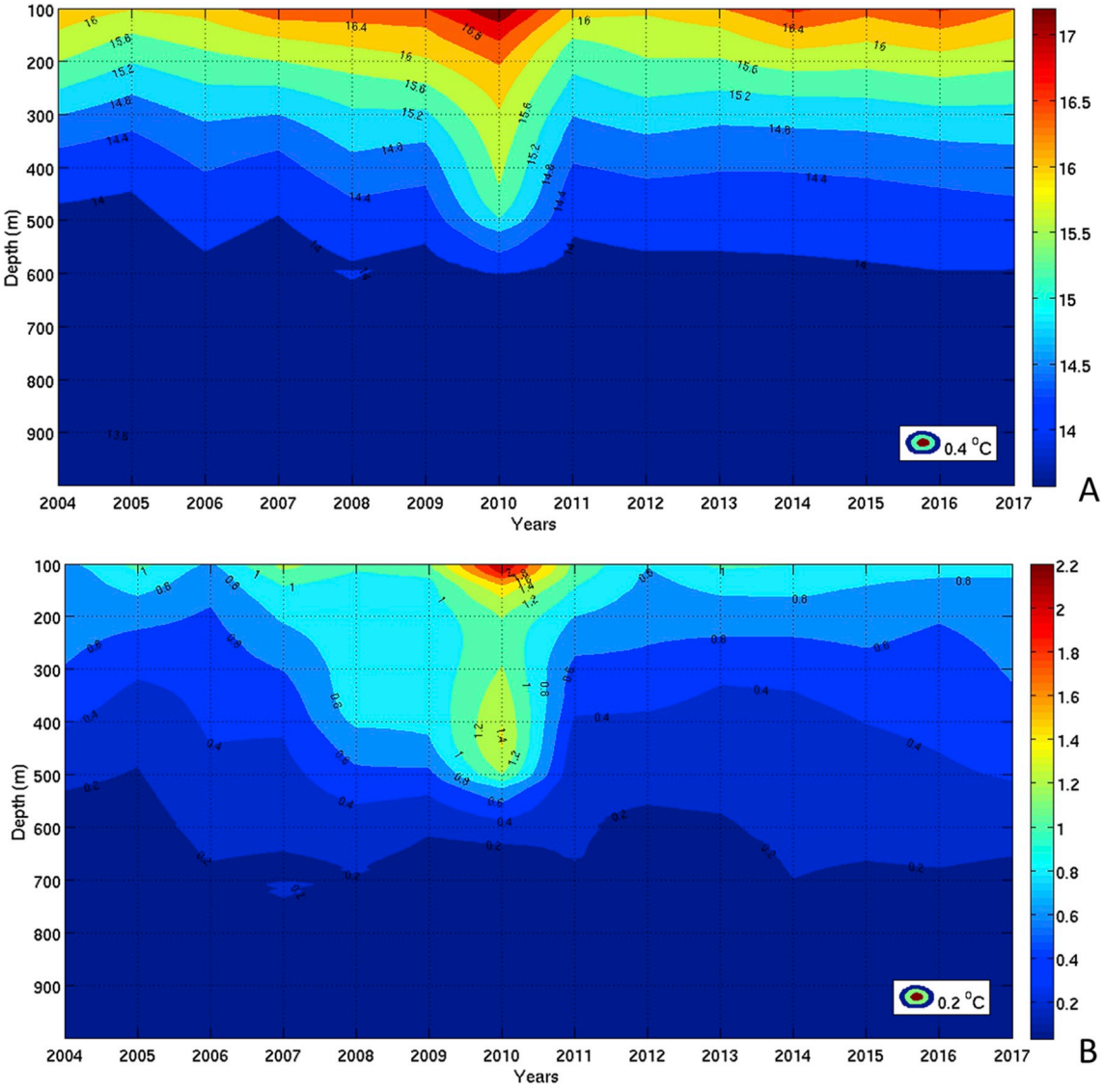

Fig. 2. Hovmöller diagram of the potential temperature yearly averaged profiles within the 100–1000 m depth zone (A) and the associated STD (B) for the Levantine and south Ionian basins during the period 2004–2017.

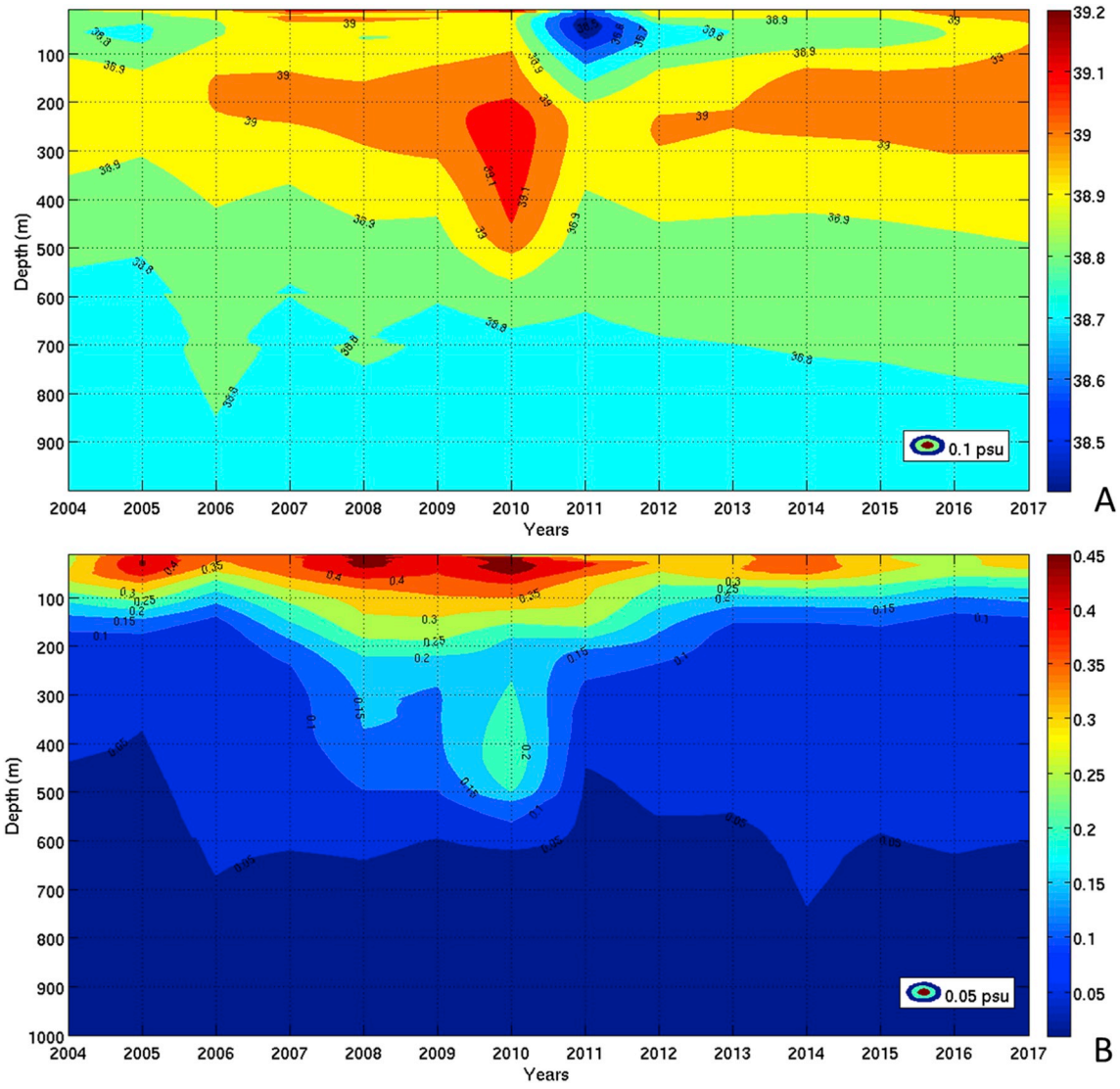

Fig. 3. Hovmöller diagram of the salinity yearly averaged profiles within the 5–1000 m depth zone (A) and the associated STD (B) for the Levantine and south Ionian basins during the period 2004–2017.

Mediterranean (Fig. 4). The Levantine Sea presents the highest surface salinity values associated with the strong presence of LSW in the area. The all-years average reaches a maximum of 39.17 psu in the eastern, and 39.15 psu in the western part. Strong LSW signal is also recorded in the Aegean Sea, with a maximum average of 39.12 psu. In the sub-surface layers the presence of AW is evident in the Ionian Sea with the strong signals in the southern (minimum average 38.66 psu at 40 m), and northern part (minimum average 38.69 psu at 42 m). A weak, but existing, signal of AW is also traced in the Levantine, with its core being deeper than that of the Ionian (38.93 at 61 m in the western Levantine). In the surface layers of the southern Adriatic area, low salinities dominate, with average values of 38.42–38.63 psu in the first 10 m whilst in the underlying layers, salinity increases gradually to reach an average maximum of 38.9 at 191 m depth. Apart from the Adriatic, the LIW core is clearly present in all the sub-regions at various depths (Fig. 4). In the northern Ionian, the western Levantine, and the eastern Levantine, it appears in the depth zone of 180–210 m, whilst in the southern Ionian, it appears deeper in the 230–280 m depth zone. In the south Aegean area, the LIW core is identified well above 200 m. In general, the southern Aegean presents the warmest and most saline waters in the intermediate and deep layers of the water column. Below 1000 m, for both the Aegean and Adriatic Seas an abrupt decrease in both *T* and *S* is recorded in the few available deep profiles in these areas (almost 10% of the total). The scarcity of data in these depths explains the considerably large salinity gradients depicted on the averaged profiles. In the Levantine and Ionian, the deep records are considerably more, reaching approximately 16% of the total. Below the 1200 m depth horizon the Levantine waters are found saltier and warmer in contrast with the Ionian waters (Fig. 4). However, for these depths, the uncertainties are considerably higher again due to the aforementioned scarcity of the available data.

The findings regarding both OHC and OSC in the Eastern Mediterranean indicate a positive trend that reflects the general increase of heat and salt within the 10–1000 m layer during the whole period of study. This increase is separated into two main periods: the first during 2004–2008, and the second during 2011–2016. An interim period (2008–2011) is also acknowledged, during which an anomaly in the variability of both thermohaline properties is observed (Figs. 5 and 6). These three periods should be interpreted separately since they integrate profile data from different sub-regions and consequently, thermohaline attributes of certain areas dominate. This is particularly true for the period before 2010, when data from Adriatic and Aegean are not included. Accordingly, the third period can be considered more representative for the whole Eastern Mediterranean area. However, it is of importance to notice that the averaged OHC and OSC along with the

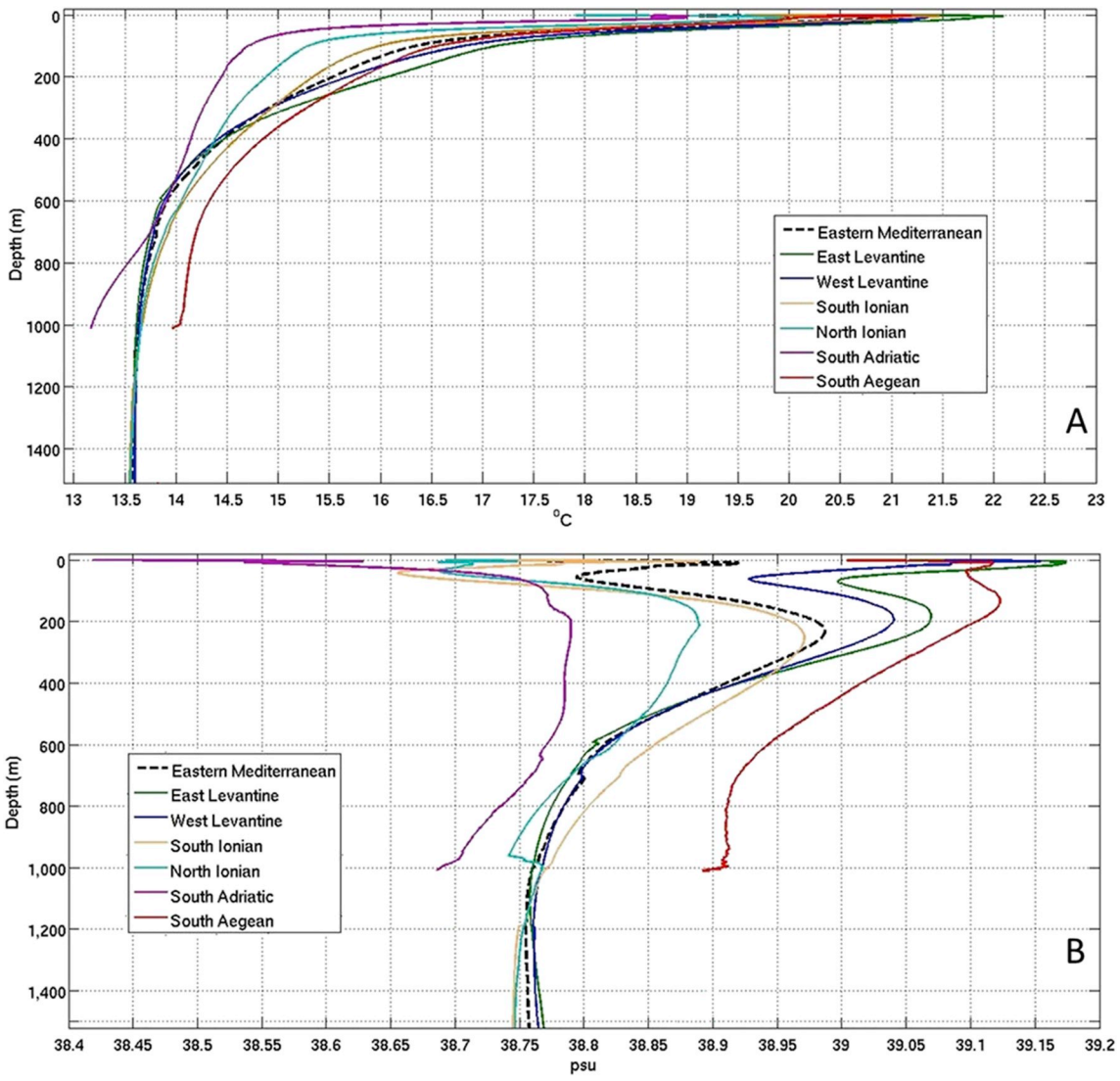

Fig. 4. Average profiles of potential temperature (A) and salinity (B) per examined region for the 14-year period (2004–2017).

estimated trends in these graphs are only indicative due to the unequal spatiotemporal distribution of the profiles. Thus, a further analysis on each sub-region including the individual profile data has also been performed and will be presented hereafter. During the first period, both OHC and OSC reach a peak, which is predominantly attributed to the heat and salt content increase of the eastern Levantine deep-intermediate layers. From 2005 to 2010, the eastern Levantine shows an increase of the stored heat that reaches approximately 0.47×10^{10} J m^{-2}, whilst a similar increase is shown in the salinity field especially for the intermediate layers (Figs. 5–8). For the Levantine and Ionian Seas, until 2008, the deep-intermediate layer (500–750 m) appears to have been the major contributor to the observed increase (Figs. 5–9). Especially during 2008, the heat content in this layer reaches its maximum (1.55×10^{10} J m^{-2}) and has a positive anomaly of 1.26×10^{9} J m^{-2} based on the average of the 14-year period (Fig. 5). The second maximum depicted in 2010 also reflects an increase of the heat content, especially in the Levantine. This maximum is lower than that of 2008, due to the fact that in 2010 profiles from Adriatic are introduced, representing almost 12% of the yearly profile dataset (Table 1). Both in the 2008 and 2010 cases, the increased stored heat and salt is mainly depicted in the intermediate layers reflecting increased LIW production in Levantine basin (Figs. 7–9). After 2010, the OHC of the wider area depicts a sharp decrease recorded in all the examined sub-regions. However, after 2011 and up until 2017, the OHC presents a weak positive trend with small inter-annual variations both in the whole area and in the examined sub-regions (Figs. 5 and 7). According to the analysis of the different depth zones, it seems that this trend is particularly evident in the deep (750–1000 m) and deep-intermediate (500–750 m) zones during 2011–2016 (Fig. 5). However, the intermediate zone (250–500 m) seems to have the strongest contribution to the total heat of the water column.

The OHC anomaly based on the 14-year average is positive during the years 2008–2010 and 2014–2016, however, for the OSC a strong variability is observed for the years up until 2011 in all depth zones (Figs. 5 and 6). After 2013, the salt increase in all the examined layers results in a positive trend (Fig. 6). Regarding the sub-regions, a gradual increase of the surface and subsurface salinity is observed during 2009–2012 in the Ionian, western Levantine, and Adriatic (Fig. 9 A, B). After 2014, a general increase of the salinity in the upper layers is recorded in all sub-regions. In the 200–350 m depth layer, both temperature and salinity are high, especially in the Levantine, reaching peaks of 16.91 °C and 39.292 psu accordingly in 2010 in its eastern part. In the Adriatic, the average salinity spans from 38.7 to 38.8 psu, except for 2011 when an abrupt decrease is recorded, that is also traced in the temperature field (Figs. 8 A, 9 C). In the same layers during the study period, the South Ionian shows the least variability with weak positive

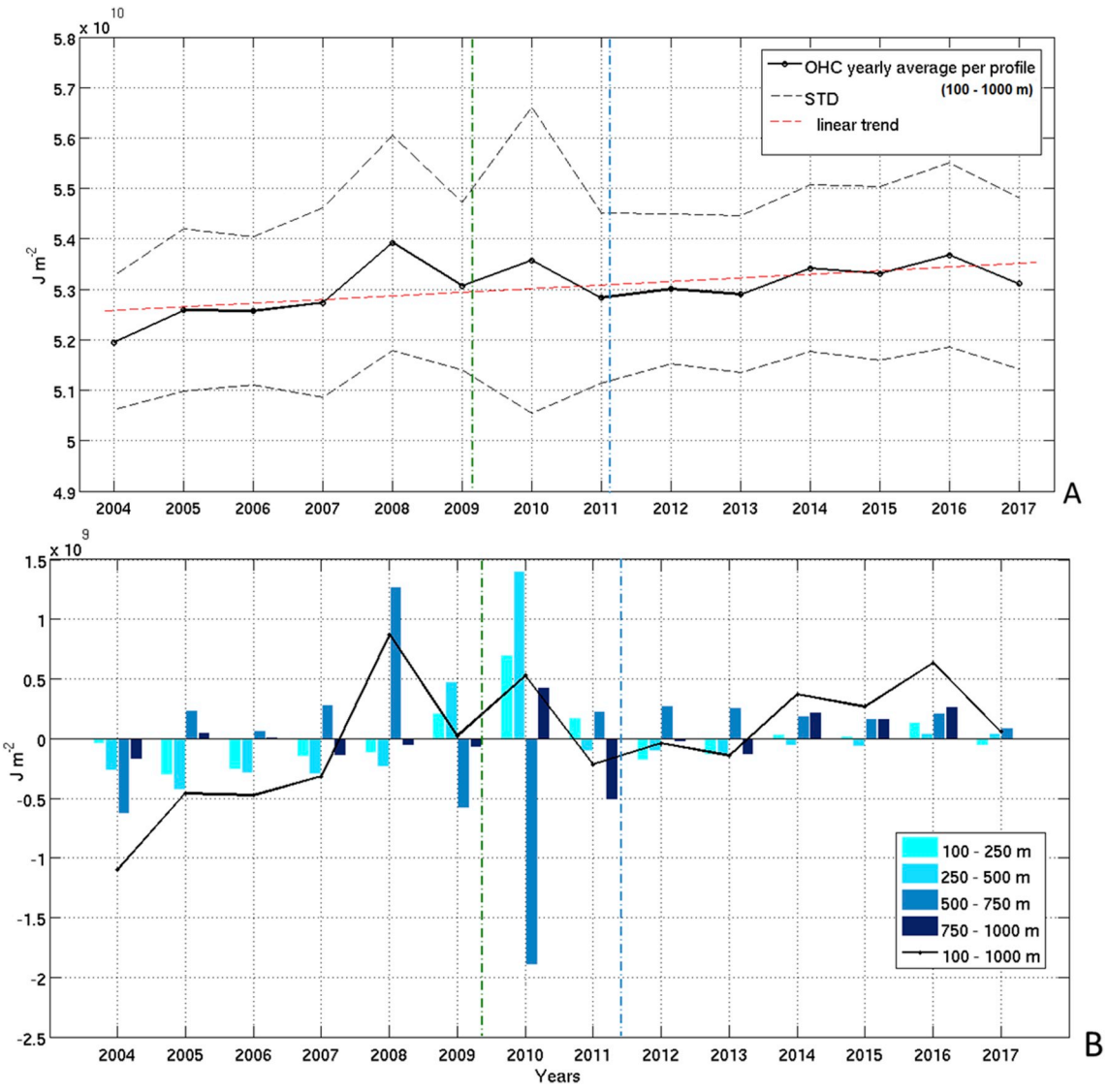

Fig. 5. Ocean Heat Content (OHC) yearly average per profile in the 100–1000 m depth zone (A) and heat content yearly anomaly per discrete depth zone and total based on the examined dataset (2004–2017) average (B). The green and blue dash-dotted lines mark the periods when data coverage changes in the various sub-regions. Until 2009 only Levantine and Ionian are represented, within 2010–2011 Aegean and Adriatic are introduced, after 2012 profile density is significantly increased and all sub-regions are represented. (For interpretation of the references to colour in this figure legend, the reader is referred to the Web version of this article.)

trends in both properties in the intermediate and deeper layers (Figs. 8 and 9).

In general, the average temperature and salinity data from the deep-intermediate (450–650 m) and deep layers (800–1000 m) present a positive trend in all sub-regions, apart from the south Aegean where a sharp decrease is recorded during 2011–2015. This decrease exceeds 0.58 and 0.64 °C for potential temperature and 0.17 and 0.19 psu for salinity in the two depth-zones respectively (Fig. 8B and C & 9 D, E). However, especially in the deep layers, salinity increases in all sub-regions after 2015.

For the investigation of the salt spatial distribution in the Eastern Mediterranean, data from each profile, at 3 separate depths, are plotted with a focus on the locations and years where salinity is recorded outside certain thresholds indicative of the main water masses in the area (Fig. 10). In Fig. 10 A, B, C, D, the biennial evolution of the horizontal sub-surface (20 & 50 m) salinity gradients is presented. These gradients indicate the areas dominated by strong LSW presence (>39.1 psu) (Fig. 10 A, B), and strong AW presence (<38.8 psu) (Fig. 10 C, D). A strong AW presence is mainly recorded in the south Ionian basin with an extension towards both the north (south Adriatic), and to the south-east towards the south-western Levantine area. During the first years of study, the AW signal is recorded stronger in the Levantine where, especially during 2004–2005 it reaches its south-eastern boundaries. Throughout the following years, this signal is reduced and is recorded again after 2015 (Fig. 10 C, D). In the same period, the low salinity signals in the Aegean originate from the Black Sea Water (BSW) inflow in the north Aegean from the Dardanelle Straits. Meanwhile, the stronger and more extended, especially after 2012, LSW signal occupies the Levantine basin, the south and north-eastern Aegean basins, the Ionian basin and, to some extent the southern Adriatic basin (especially in the 20 m depth horizon) (Fig. 10 A, B). It is of interest to notice the similarities between Fig. 10 A, C, and 10 B, D, suggesting generally weak vertical salinity gradients in the upper layers. In the intermediate depths (250 m), the domination of LIW is apparent after 2012 in all sub-regions, apart from the north Ionian and Adriatic basins (Fig. 10 F). During the first years the LIW is mainly recorded in the Levantine occupying its south and southeastern areas, with a particular strong core south of Cyprus during 2008–2011 period (Fig. 10 E). At the 500 m and 750 m

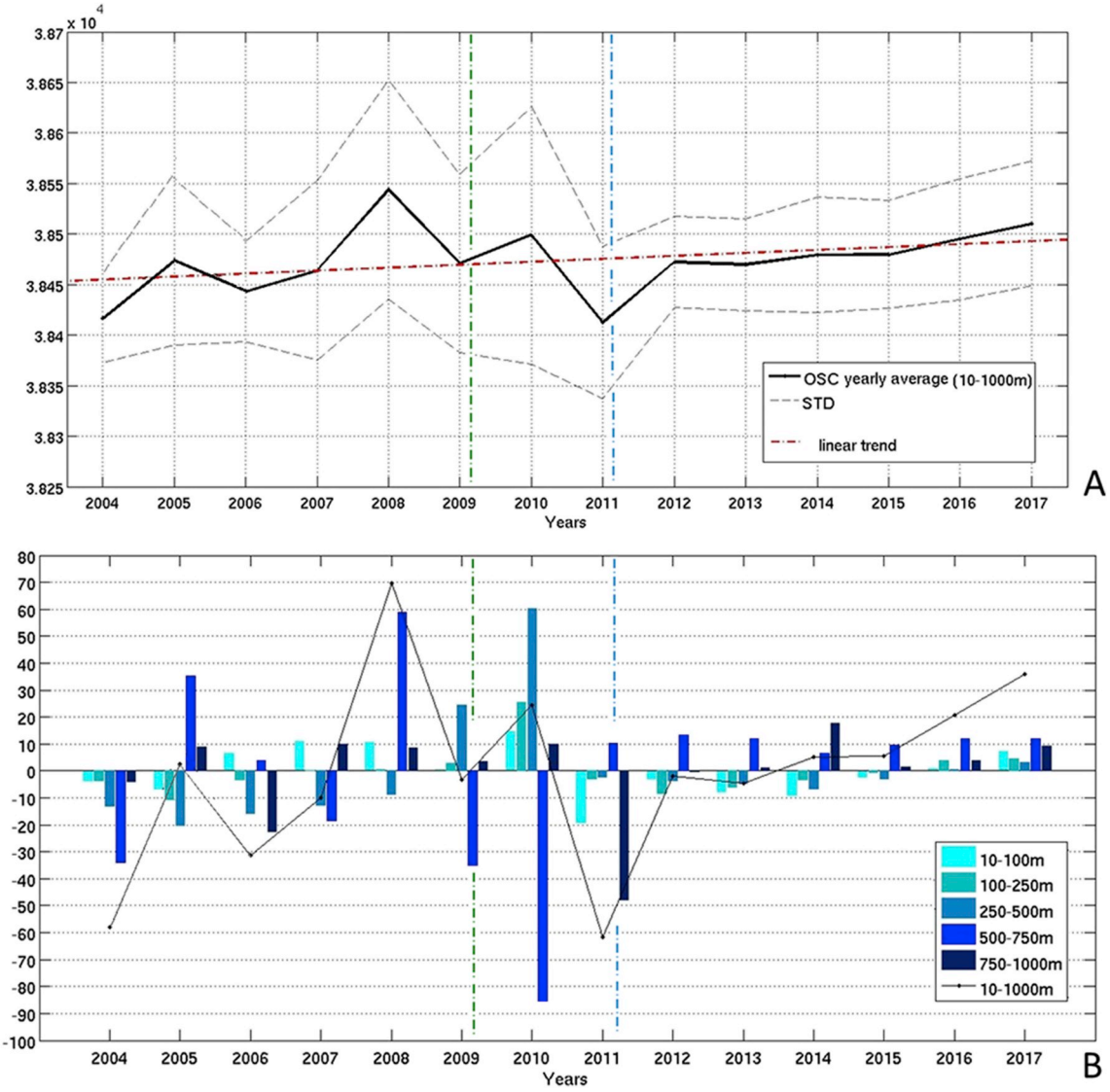

Fig. 6. Ocean Salt Content (OSC) yearly average per profile in the 10–1000 m depth zone (A) and salt content yearly anomaly per discrete depth zone and total based on the average of the examined dataset (2004–2017) (B). The green and blue dash-dotted lines mark the periods when data coverage changes in the various sub-regions. Until 2009 only Levantine and Ionian are represented, within 2010–2011 Aegean and Adriatic are introduced, after 2012 profile density is significantly increased and all sub-regions are represented. (For interpretation of the references to colour in this figure legend, the reader is referred to the Web version of this article.)

depth levels, relatively high salinities were still recorded in the Aegean and central Ionian areas whilst, in the Levantine the majority of the profiles recorded salinities less than 38.8 (however, in certain areas high and low salinities were recorded indicating strong gradients throughout the examined period). Deeper, at 1000 m and 1500 m levels, the majority of the salinity values were below 38.75 psu. Nevertheless, in certain areas such as Aegean, central Ionian, and northern Levantine, salinity values exceeded 38.8 psu.

To investigate the aforementioned long-term trends of heat and salt fluxes in the Eastern Mediterranean, the *T-S* variability in the eastern Levantine and south Ionian is further examined as these two sub-regions have the densest profile coverage over time. The associated *Theta-S* diagrams at discrete depth layers over the years, highlight the previously presented variability and the shift of the thermohaline properties during different periods. In general, a biennial temporal classification was chosen with the exception of 2008–2010 and 2011 periods, which were plotted separately due to their previously stated distinct characteristics. In the sub-surface zone (40–60 m) the shift of the *T-S* values describing primarily the AW, and secondarily the LSW, variability is apparent after 2006 when, in both areas, the colder and fresher water masses are replaced by water masses with higher *T-S* values (Fig. 11 A, B). Especially in the Levantine, this shift is clearer, with 3 discrete salinity cores representing the time periods of 2004–2005 (cyan dots), 2006–2007 (blue dots), and 2008–2010 (light green dots). In 2011 (green dots), salinity is more evidently reduced in the Ionian but rises again in the following years, reaching its higher values during 2012–2013 (yellow dots), and 2016–2017 (red dots). In the 200–300 m depth layer (Fig. 11 C, D), a warming and salinization is also apparent in the Levantine after 2006, reflecting the increased LIW production in the eastern part that had already started in early 2007, and reached a peak in 2010. This signal is captured in the Ionian only after 2008 and becomes stronger in 2011. During the following years, temperature and salinity rise in the intermediate layers of the Ionian, with the highest salinities being recorded after 2013, whilst in the eastern Levantine, the salinity peak is recorded during the 2008–2010 period (Fig. 11 C, D, E, F). Signals of denser water masses are recorded in both areas after 2016. This is more evident in the deep intermediate layer (500–600 m) where water masses of 2016–2017 exceed the 29.23 kg m^{-3} isopycnal (Fig. 11 E, F).

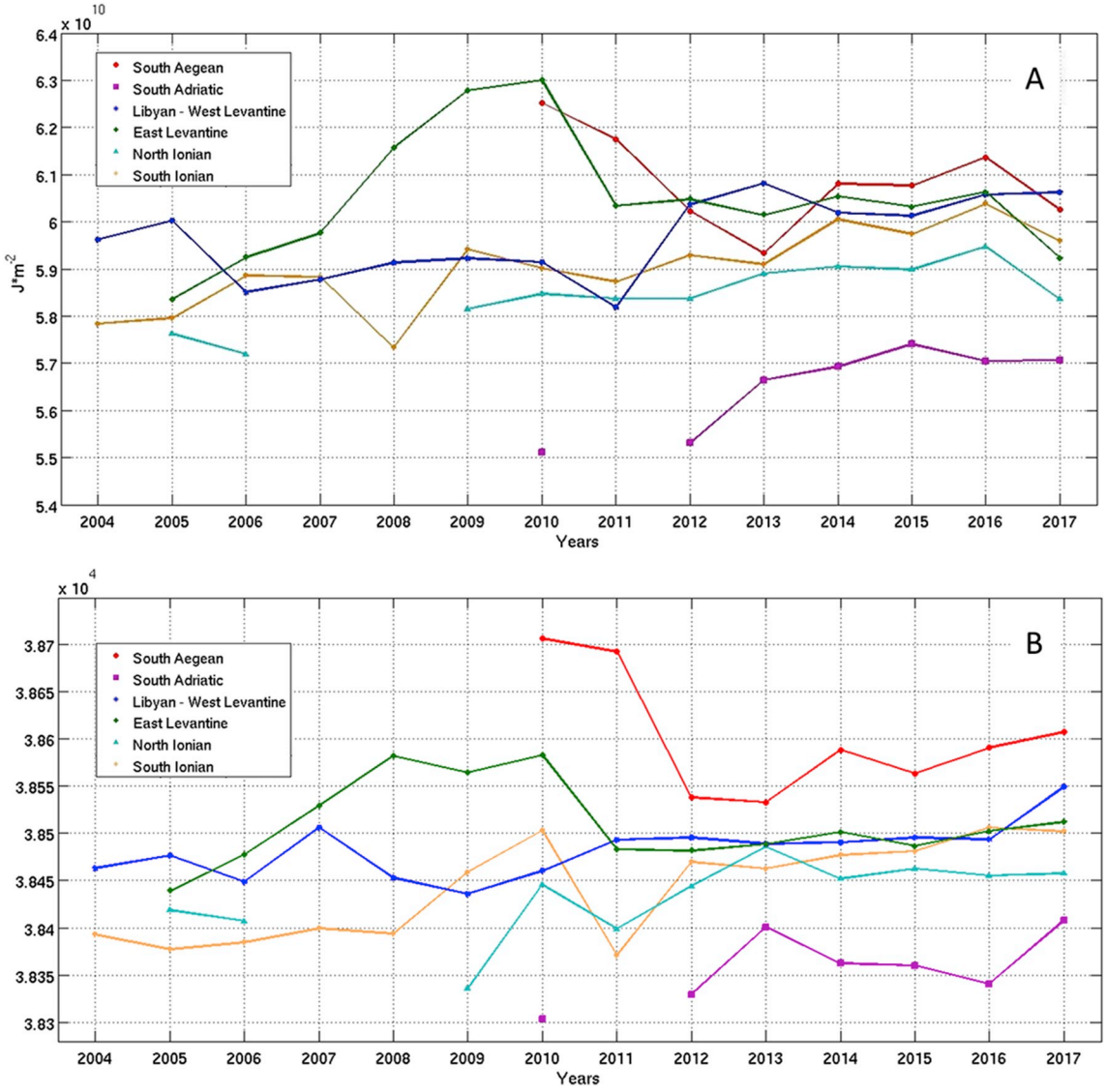

Fig. 7. Ocean Heat Content (OHC) yearly average per profile in the 100–1000 m depth zone (A) and Ocean Salt Content (OSC) yearly average per profile in the 10–1000 m depth zone (B) for each examined sub-region.

However, this period is also characterised by the coexistence of less dense water masses that were not recorded previously. Especially for the Ionian, this density heterogeneity mainly derives from the large span of the salinity field (38.6–39.1) (Fig. 11 E) indicative of the co-existence of LIW/CIW and TW during these years in the area.

For the wider Eastern Mediterranean area, the potential density (σ_θ) field was also estimated based on all the available profiles. In the upper layers, dense water (>29.0 kg m^{-3}) is recorded mainly in the Adriatic and the central-north Levantine. The locations where relatively dense surface water is recorded (σ_θ > 28.8 kg m^{-3}), and not recorded (σ_θ < 28.6 kg m^{-3}), during the winter early spring period (January–April), have been identified (Fig. 12 A, B). Especially during the first period, dense surface water is noted in the Rhodes Gyre area, and the Aegean Sea (Fig. 12 A). The latter does not present dense surface water from 2011 to 2016. During these years, and until 2017, it is mainly the Adriatic and the Ionian basins where dense surface water is found along with the northeastern Levantine area (Fig. 12 B). This spatiotemporal variability of the surface density field reflects, apart from the aforementioned salt distribution with regards to the AW and LSW presence, the areas where DWF events are expected to occur. With regards to these graphs, it is of interest to notice the low-density surface core at the Shikmona anticyclonic system south of Cyprus, an area where high salinities are present (Figs. 10 A, & 12 A). This pattern also appears in the 250 m depth horizon (Fig. 10 E, F, & 12 C, D) reflecting the strong warm LIW core recorded in the Levantine during the 2006–2010 period (Fig. 11 D, F). The pattern of high salinities – low densities is also observed, mainly after 2012, in the areas of the Ierapetra and Pelops Gyres south-east and west of Crete accordingly. In general, at the 250 m depth horizon, dense water masses (>29.1 kg m^{-3}) are recorded in the north-central Levantine, in the Cretan Cyclone south-west of Crete, in the north Aegean and the south Adriatic areas (Fig. 12 C, D). In the latter, high and low densities co-exist at all examined depth levels. Moreover, dense water masses at 500, 750, 1000, and 1500 m are spatially distributed in the Aegean, south Ionian, and Levantine basins.

The strong spatio-temporal density gradients depicted from the analysis, reflect the basins thermohaline circulation and DWF processes that are associated with intense mixing in the water column. To identify the areas where such processes took place, a further analysis on the dataset was applied which investigated MLD and BVF estimations for each profile. Accordingly, the locations of the winter – early spring period (January–April), that depict MLDs deeper than 150 m and shallower than 100 m, were identified and temporally sorted (Fig. 13).

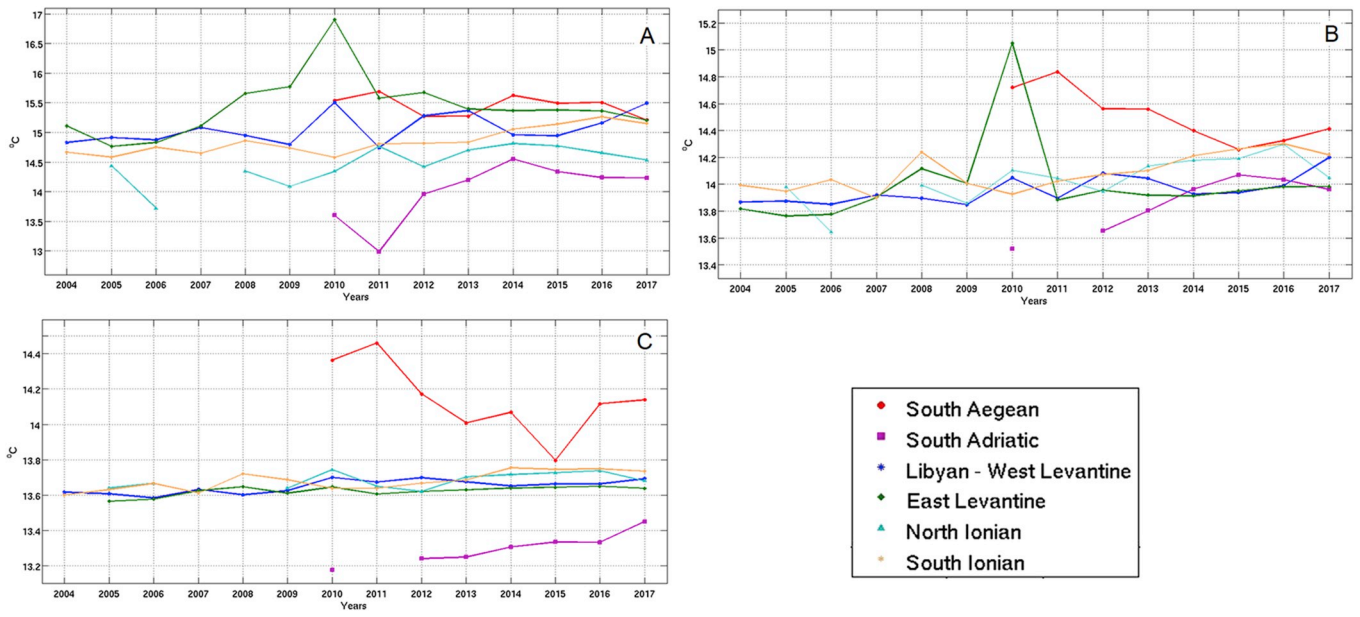

Fig. 8. Yearly average potential temperature per depth zone per region for the period 2004–2017. Depth zones: A: 200–350 m, B: 450–650 m, and C: 800–1000 m.

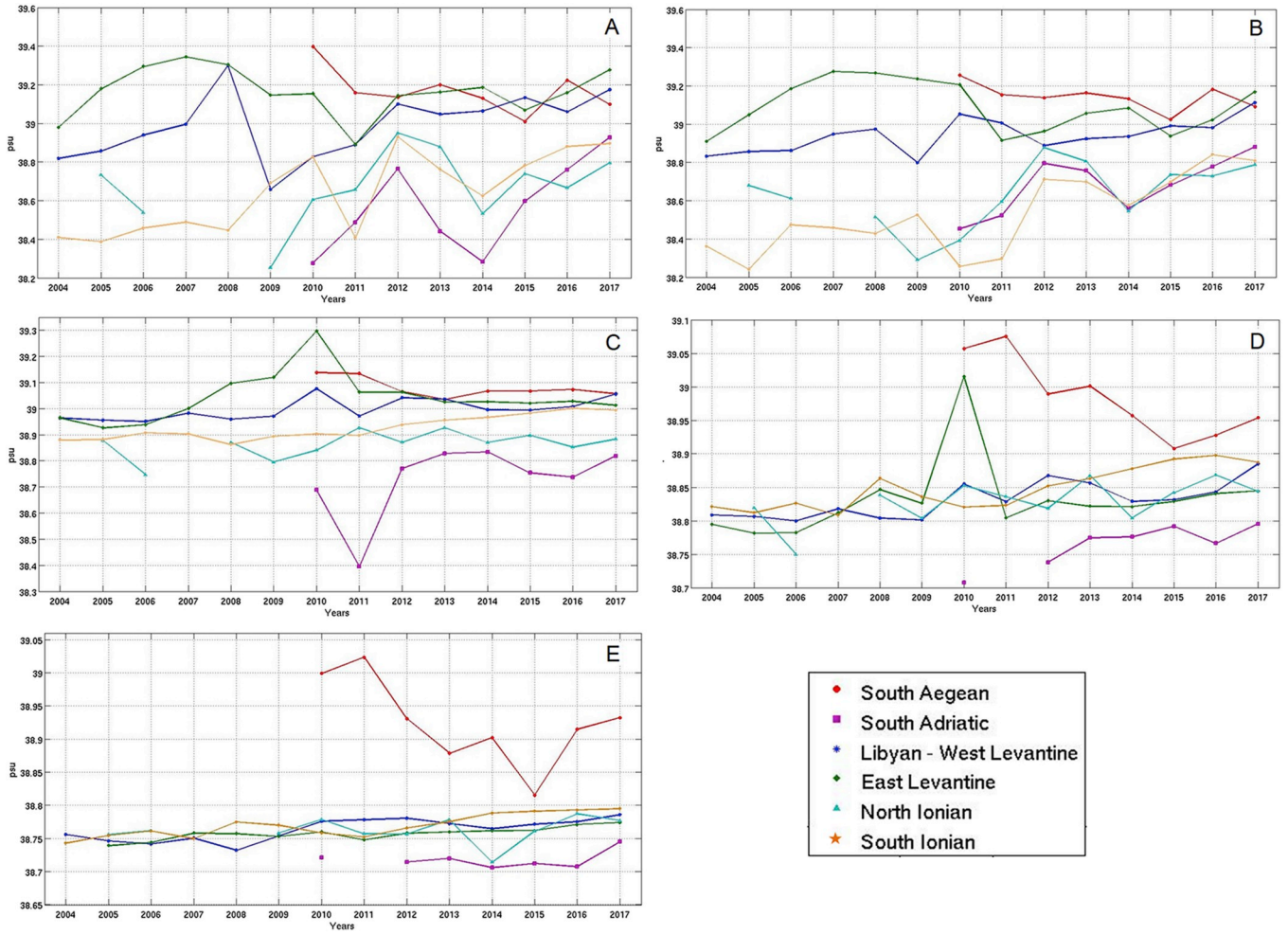

Fig. 9. Yearly average salinity per depth zone per region for the period 2004–2017. Depth zones: A: 5–15 m, B: 20–60 m, C: 200–350 m, D: 450–650 m, and E: 800–1000 m.

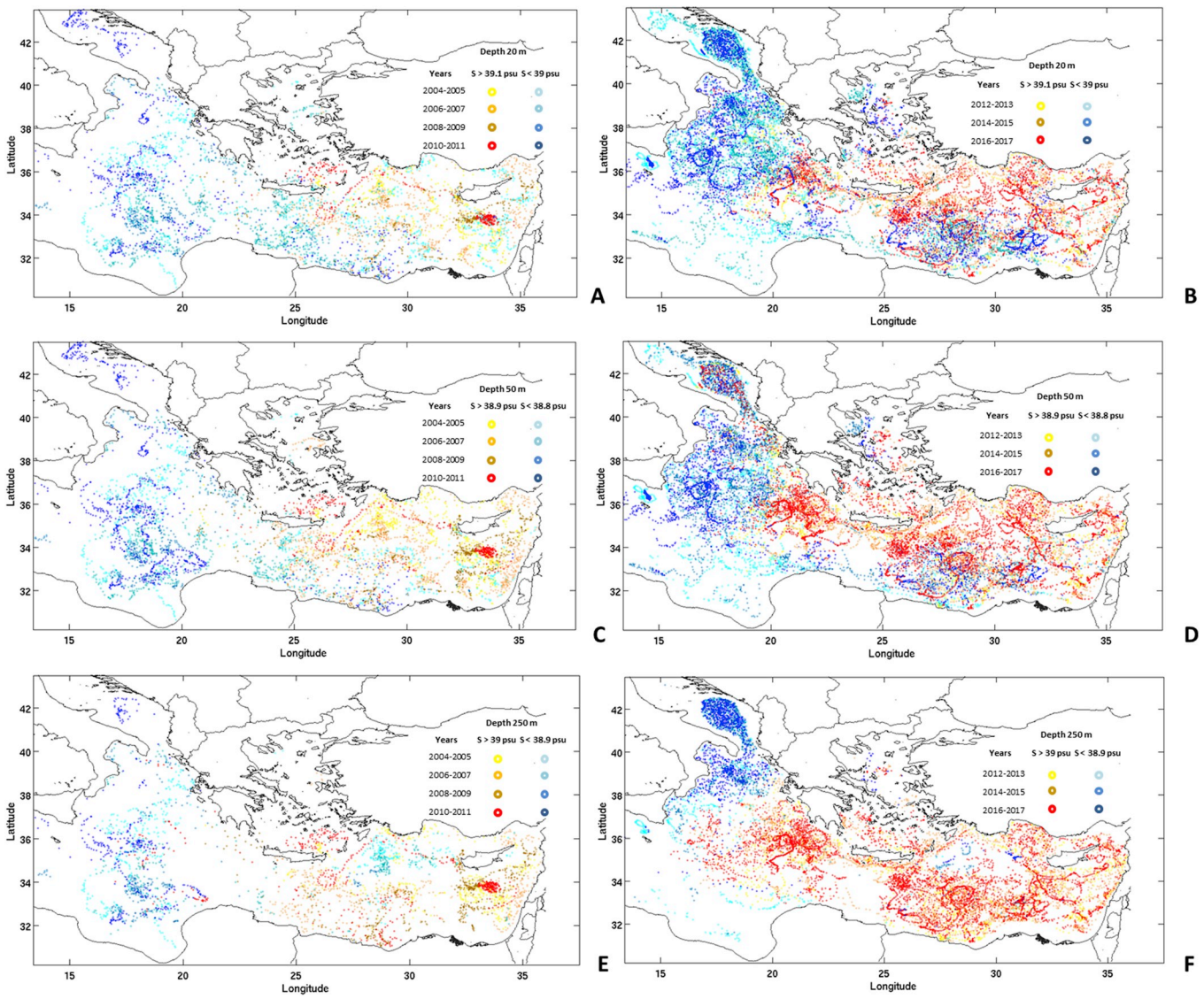

Fig. 10. Spatiotemporal distribution of salinity values recorded from Argo profilers in the Eastern Mediterranean. S < 39 and S > 39.1 at 20 m during 2004–2011 (A) and during 2012–2017 (B), S < 38.8 and S > 38.9 at 50 m during 2004–2011 (C) and during 2012–2017 (D), S < 38.9 and S > 39 at 250 m during 2004–2011 (E) and during 2012–2017 (F).

During the first years of the study period, deep homogenisation is observed in the Levantine a) in its northern, and b) central and south-eastern parts. Although both reflect the occurrence of convection events, the former represents convection of less dense water as shown from the density field (Fig. 12 A, C, & 13 A). This results in the presence of the warm low-density LIW core in the area during 2006–2010 (Fig. 11 D, F). After 2011, the south Adriatic, central Ionian, Aegean, central Levantine, and eastern Levantine, are the main areas where the deepest homogenisation of the water column is depicted (Fig. 13 B). In the Adriatic the majority of events were found during January–February whilst, in the Ionian, Levantine and Aegean the most records are depicted during late February–March. It is important to note that although all these areas represent cases of low vertical density gradient, not all present deep convection due to their relatively low-density field. Such cases are the Pelops and Ierapetra Gyres where in contrast with the Adriatic and north Aegean cases, the ventilation reached considerably deeper. In general, the majority of the events are measured after 2012, however, caution should be applied to these results as during the 2004–2011 period, the available profiles were sparse, and sub-regions like Aegean and Adriatic have minor or no representation at all. In many areas, where deep homogenisation was recorded, the estimated BVF was found to be negative within the first 100 m of the water column. Although a single BVF profile reflects short time scale instabilities, the fact that such events were captured in deep MLD areas can be an indicator of convection events. The combination of both information is an indicator of the wider areas where intense vertical instabilities were recorded during the examined period. It is interesting to notice that many of such cases (ex. south Adriatic, Libyan Sea, south of Cyprus, etc.) are also areas where strong salinity and density temporal variability is observed in the deep intermediate layers.

4. Discussion

The Argo profiles dataset examined in this study has been proved a valuable source of information regarding the area's physical properties distribution. However, the high spatio-temporal variability of the available profiles induces uncertainties, especially during the first years of the examined period when the profiles were sparse. Recent studies (e.g., Jordà et al., 2017) have dealt with this issue with interesting results, however, the above authors accurately make a note of caution that is required regarding the interpolation of the discrete data on a regular grid to reduce the impact of the heterogeneous spatial distribution. In

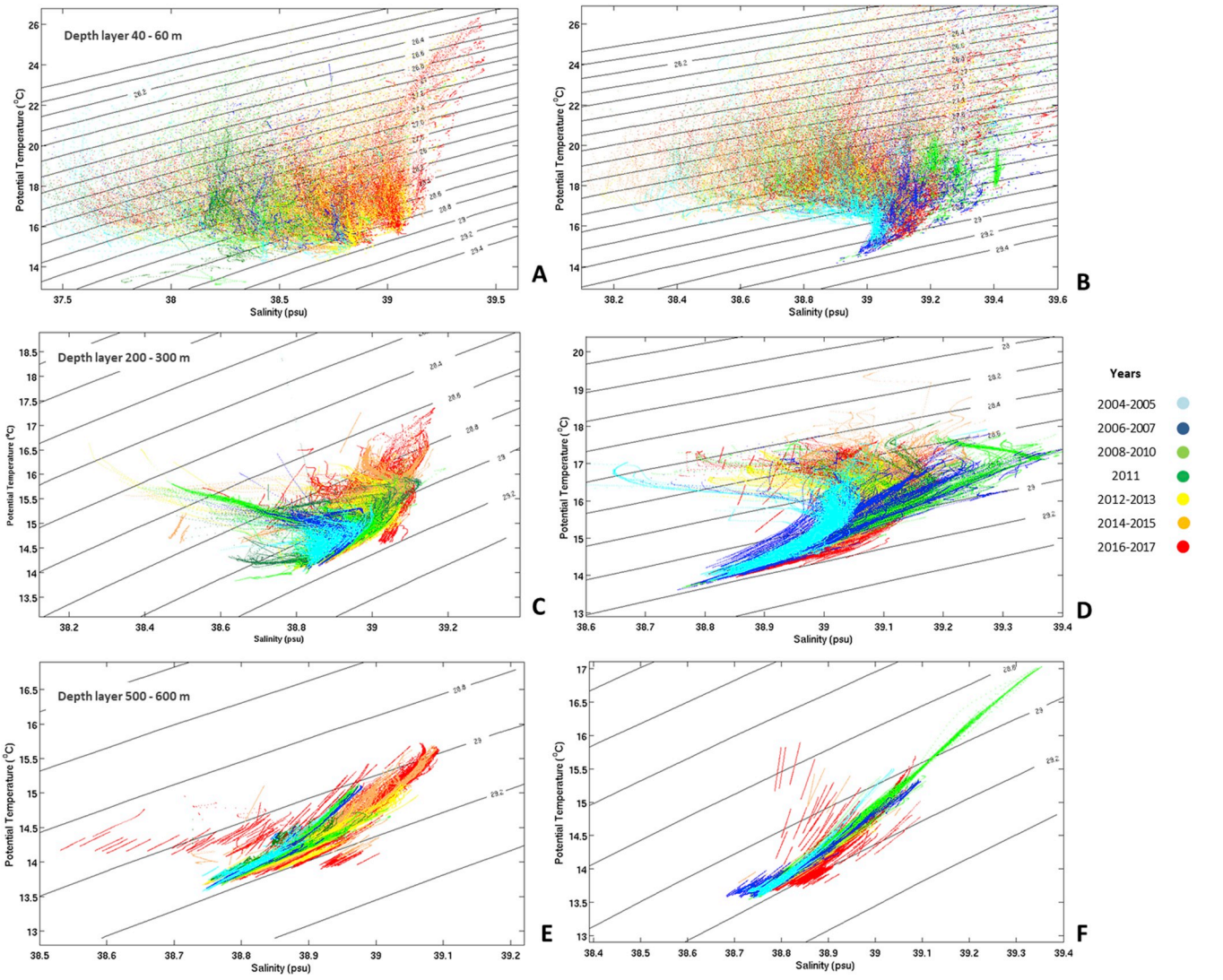

Fig. 11. Theta-S diagrams from Argo profiles per year and depth zone during 2004–2017 in the south Ionian and eastern Levantine Mediterranean. A: South Ionian at 40–60 m, B: Eastern Levantine at 40–60 m, C: South Ionian at 200–300 m, D: Eastern Levantine at 200–300 m, E: South Ionian at 500–600 m, Eastern Levantine at 500–600 m.

this analysis, apart from spatial, there is also temporal heterogeneity. Thus, having acknowledged the uncertainties and misinterpretations induced due to the spatio-temporal inhomogeneity of the dataset, this study mainly focuses on examining the actual recorded field values, avoiding extended statistical classifications and data interpolation and extrapolation methods that can produce unknown errors dependent on subjected analysis choices and arbitrary selected parameters.

From the data analysis, important information is extracted, and synthesized, regarding the Eastern Mediterranean recent hydrographic picture. In the upper layers, the low salinity signal associated with the presence of AW presents intense spatio-temporal variability. Data from individual profiles also revealed inter-annual variability of the northward and eastward paths of AW through the Ionian Basin. The AW eastward path appears to penetrate far eastwards during 2004–2005, and after 2016, whilst presenting limited penetration in the 2006–2010 period (with an exception of the south-western Levantine area where its core is found deeper). The absence of AW especially in the Levantine basin after 2005, and until 2010 resulted in the salinity increase of the upper layers favouring the aforementioned DWF events that were reported in the area during the winter – early spring periods of 2007–2010. In 2011, AW is recorded stronger in the eastern sub-regions (Levantine, south Aegean), whilst salinity rises in the northern Ionian and Adriatic parts (Fig. 9 A, B) preconditioned the latter for DWF events that are traced after 2012. In the following years, the AW presence is reduced in all sub-regions until 2016, except for the Ionian and Adriatic during 2014. It is of interest to note the agreement of the presented AW variability, with the previously reported alternation of the basin's general circulation pattern. More specifically, the weakening of the southeast AW inflow coincides with the anticyclonic mode of the North Ionian Gyre (NIG) during that period (Gačić et al., 2014). However, in 2011, the observed strengthening of the AW signal coincides with the cyclonic reverse of the NIG. This led to the surface salinity increase in the north Ionian – Adriatic which reached a peak in 2012, as previously reported (Kassis et al., 2017) when the NIG was reversed again due to extreme winter conditions that year (Gačić et al., 2014). On the contrary, the high salinity signals in the subsurface zone, which are mainly associated with LSW, appear more extended. Especially after 2010, LSW occupies the Levantine, Aegean, and the central part of the south Ionian basin. In the eastern Levantine, the maximum sub-surface salinity increased from 2004 up until 2007. According to Kress et al. (2014), this increase started in 2005 and lasted until 2010 affecting the upper and intermediate layers down to 300 m. In this study, the sub-surface salinity increase for the whole Levantine is estimated to last until 2008 and starts again after 2011. For the underlying layers, this increase is found from

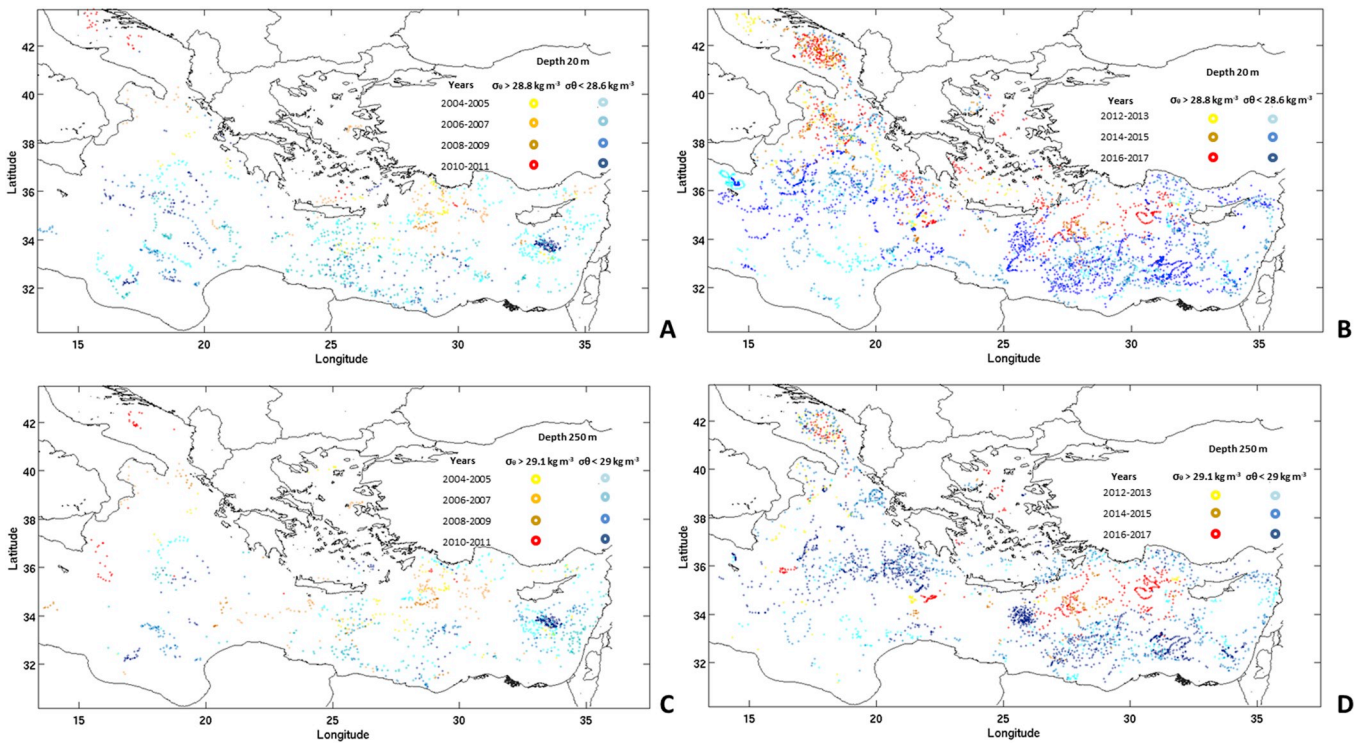

Fig. 12. Spatiotemporal distribution of potential density (σ_θ) values recorded from Argo profilers in the Eastern Mediterranean during January–April. $\sigma_\theta < 28.6$ kg m^{-3} and $\sigma_\theta > 28.8$ kg m^{-3} at 20 m during 2004–2011 (A) and during 2012–2017 (B), $\sigma_\theta < 29$ kg m^{-3} and $\sigma_\theta > 29.1$ kg m^{-3} at 250 m during 2004–2011 (C) and during 2012–2017 (D).

2004 up until 2010. In Ozer et al. (2017) the LIW peak in 2008 has been also reported and is associated with the contemporary anticyclonic phase of the NIG. In this analysis, a dramatic salinity increase is traced from the 200 m level down to 750 m (Figs. 3, 9 and 11) in the eastern Levantine reaching a peak in 2010, it is followed by considerably lower values in the proceeding years. This variability has been also reported in Krokos et al. (2014), where a salinity increase of almost 0.3 psu is described during 2005–2010 in the upper 300 dbar layer of the easternmost part of the Levantine, that is followed by a relaxation period during 2011 and 2012. From the analysis of the Theta-S diagrams, it seems that the high surface salinities of that period led to LIW formation that reached the deep intermediate layers. Due to this process, relatively warm and thus less dense ($\sigma_\theta < 29$ kg m^{-3}) water masses are depicted below the depth horizon of 500 m (Fig. 11 F). In the following years, denser water masses dominate the area at depths that exceed the 29.2 kg m^{-3} isopycnal (Fig. 11 E, F). Strong signals of Levantine waters are also recorded in the southern Adriatic after 2012. The inflow of LSW and LIW in the Adriatic is also indicated in previous studies as being associated with the cyclonic mode of the NIG (Gačić et al., 2010). During that mode, the northward transport within the south Ionian upper layers along the Hellenic Trench is favoured, resulting in the inflow of LSW and LIW into the Otranto Straits (Kassis et al., 2017). In general, the LIW signal is apparent in all sub-regions during the whole period of study, apart from the year 2011 in the Adriatic. Its core is deeper in the South Ionian, and shallower in the north and south Aegean. The LIW signal undergoes a second increase after 2014 in all sub-regions, apart from the Aegean where its strong presence in 2010 and 2011 becomes gradually weaker in the following years. The highest salinity signal observed in the 500–750 m layer was recorded in the south Aegean during 2010–2011 period (Fig. 9 D), likely associated with Cretan Intermediate Water (CIW) that was previously produced from DWF events that took place in the area (Kassis et al., 2015; Schroeder et al., 2013). The abrupt salinity decrease that follows after 2012 has also been reported in previous studies (Kassis et al., 2016), and reflects a dramatic change in the hydrographic picture of the south Aegean basin. During 2013–2014, significantly fresher and slightly colder water masses occupied the layers below 100 m. The absence of strong LIW and CIW signals was attributed to an intensified outflow of these water masses from the Cretan Straits. At the same time, Transitional Mediterranean Water (TMW) entered the basin compensated for the outflow. The presence of TMW had been reported in the basin since 2012, and such presence can act as a tracer for DWF events in the Aegean Sea (Velaoras et al., 2015).

In the overall area of study, the temperature variability, especially in the intermediate layers (200–600 m), is relatively similar to the variability of the salinity field. In 2005, the first increase of both *T-S* properties at the intermediate layers is observed, but especially after 2007, both properties abruptly increase in the deep-intermediate zone (Figs. 8 and 9). The warming and salinization of these layers is mainly recorded in the Levantine in 2008 and 2010, and reflect: a) the aforementioned strengthening of the LIW signal due to increased LIW production mainly in the eastern part as has previously been reported (Kress et al., 2014; Ozer et al., 2017) and, b) the increased production of CIW/LIW and the outflow of these water masses from the Aegean Sea especially for the 2010 event (Schroeder et al., 2013; Velaoras et al., 2013). It is of interest to note that during this period, the distribution of heat and salt through the different depth zones is not homogeneous. The 100–250 m layer presents a gradual warming and salinization from 2007 until 2010. However, during 2008, it is the 500–750 m layer which accumulates large amounts of heat and salt, showing that the ventilation did not reach significantly deeper depths. In 2009, 2010, the same layer presents extended heat and salt deficit, however, in the overlying and underlying layers, the OHC is increased (Figs. 5 and 6). This indicates the occurrence of vertical mixing, especially between the 500–750 m and 750–1000 m zones, and secondary weaker DWF events during 2009. Furthermore, the significant decrease of heat and salt in the 500–750 m zone is also attributed to the low OHC-OSC of the north Ionian and south Adriatic profiles in 2009 and 2010 accordingly. In 2010, the maximum increase rate was recorded in the deep (750–1000 m) layer. In general,

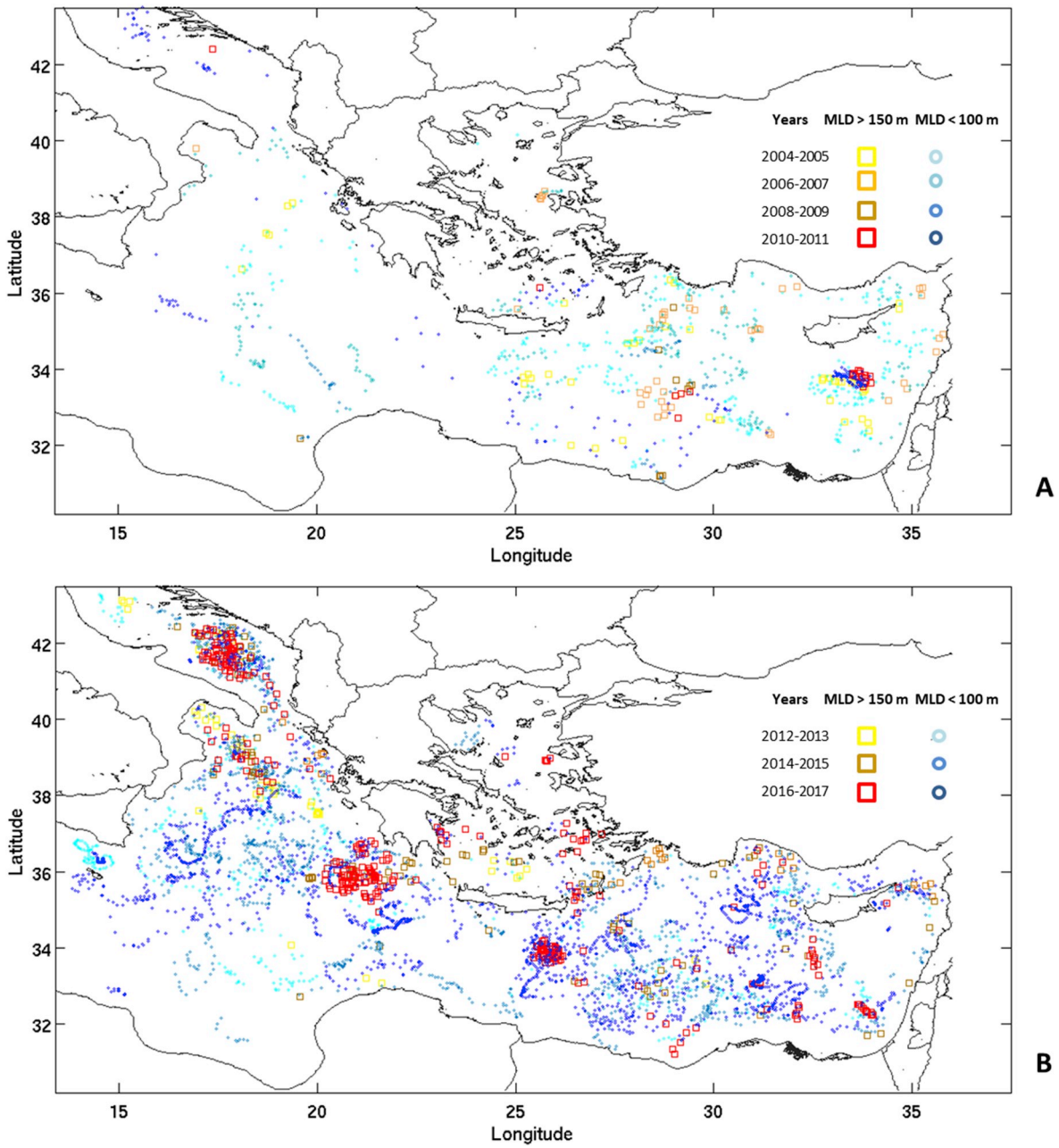

Fig. 13. Profile locations where the mixed layer depth exceeds 150 m (squares) and where is lower than 100 m (dots) for the winter – early spring periods (January–April) of 2004–2011 (A) and 2012–2017 (B).

during the 2007–2010 period, the water column below 100 m is on average, significantly saltier, and warmer. After reaching a peak during 2010 (15.5 °C on average at 300 m), in the proceeding years, the temperature in these layers is reduced, although stabilised at approximately 0.1 °C degree higher than the previous period. In 2011, a general decrease of the physical properties is depicted in the first 1000 m of the water column that is observed in all sub-regions. The observed heat deficit is the combined result of the heat transfer towards deeper layers, as depicted from the warming of the 1000–1250 m zone, the reduced DWF events, and the cold winter period of 2011–2012 that followed. Nevertheless, after 2012, a slow increase of the water column's thermohaline properties is again recorded as the DWF events are accentuated mainly in the Adriatic area. This is also recorded in the deep waters (1000–1500 m) of the whole area of study during the period 2013–2017 with a slow gradual warming and salinity increase that reached 0.05 °C and 0.02 psu accordingly.

The estimated average OHC per profile in the 100–1000 m layer in the Eastern Mediterranean, presents a total increase of approximately 0.9×10^9 J m^{-2} within the 14-year study period. corresponding to a positive trend of 0.64×10^8 J m^{-2} yr^{-1} (Fig. 5). This is translated to a total heat increase of approximately 0.126×10^{22} J for the 2004–2017 period which exceeds the estimated trends for the global ocean. A quantitative comparison with the global estimates is not possible due to the different periods analysed in various studies and the aforementioned spatio-temporal constraints. Nevertheless, it is of interest to note that the corresponding total OHC for the upper 700 m layer for the 1955–2010 period has been estimated $16.7 \pm 1.6 \times 10^{22}$ J representing a rate of 0.27 W m^{-2} per unit area of the World Ocean (Levitus et al., 2012). In similar studies (Balmaseda et al., 2013) the 1975–2009 trend is approximately 0.39 W m^{-2}, and 0.47 W m^{-2}, for the upper 700 m, and 2000 m respectively, whilst in Cheng et al. (2016), it is estimated to be approximately 0.75 W m^{-2} from 1992 to 2005. According to Von

Schuckmann et al. (2014), the Argo-based dataset analysis revealed an increase with mean rates of 0.5 ± 0.1 W m^{-2} from 2005 to 2012. In the present findings, the estimated corresponding rate for the Eastern Mediterranean basin is considerably higher for the same period. However, a less biased estimate can be derived only after 2012, when the profile coverage is more representative of the area. During that period, the energy transfer rate is estimated approximately 1.15 W m^{-2} per unit area for the upper 1000 m. Nevertheless, the uncertainty of these estimations is high since the OHC average increase lies below the confidence interval of the corresponding STD (which in this case is approximately ± 1.4 × 10^9 J m^{-2}), and the time period, in this case, is too short to provide a reliable trend. The estimation of the salt content variability has shown similar trends with the heat content. The OSC average presents a total increase of approximately 0.01 Kg m^{-2} of salt per profile. After 2011, this trend is stronger, with an approximate yearly increase of 0.0016 Kg m^{-2} per profile. However, this increase is uniformly depicted in the water-column only after 2014, since until 2013 it is attributed to the salinization of the intermediate layers as a result of the intermediate water formation events of the previous period. Especially in 2011, the previously produced water is deeper, and the 750–1000 m layer is occupied by the underlying colder and fresher water masses. This deep (>1000 m) ventilation of the Eastern Mediterranean is reflected by the slow process of the warming and salinization of the water masses that occupy the 1200–1500 m layer zone, and it is especially apparent in the eastern Levantine after 2011, and in the south Ionian after 2013. In general, the salinity spatial distribution presents an intense west – east positive gradient at the first few hundred meters of the water column. From the surface down to 400 m depth horizon, high salinities dominate in the Levantine, south Aegean, and south-eastern Ionian basins, however, this picture is alternated below that depth. Between 500 and 750 m depth, certain areas have depicted large salinity spans as a result of DWF events or horizontal advection that followed DWF events. Such examples are the south Adriatic basin, and the south Aegean – south Ionian water exchanges, accordingly. Especially in the Adriatic, such intense variability is also presented in the density field (Fig. 12), and is associated with enhanced vertical convection events during 2012–2017. On the contrary this is a relaxation period for the Aegean Sea with reduced DWF events that are mainly recorded in its central-eastern and northern parts (Figs. 12 and 13) e.g., the DFW events traced during 2016–2017 which are in agreement with Velaoras et al. (2017). In general, for certain areas where intense salinity and density variation is recorded, the MLD is also extended and depicts a deep homogenisation of the upper layers (Figs. 10, 12 and 13). However, there are areas with increased temporal variability in the salinity and density fields and strong *T-S* trends, such as LIW signals, that are not formation regions. In such areas, the newly formed water is advected from a neighbouring area (Marshall and Schott, 1999; Schroeder et al., 2017). Such an example is the central Levantine basin, where increased LIW signal is recorded however the formation process took place several kilometres north at the Rhodes Gyre area where such a signal is absent. The later seems preconditioned for DWF with increased surface salinity during the whole study period and depicts dense intermediate water as shown from the σ_θ distribution.

In general, the warming and salinization depicted from the present analysis is in agreement with previous studies concerning the Mediterranean area. Such an example is Schroeder et al. (2017) in which the investigation of the intermediate water thermohaline properties that enters Eastern Mediterranean through the Sicily Channel has shown strong increasing trends of temperature and salinity, especially after 2011. These trends are stronger than those reported at intermediate depths in the global ocean. The driving mechanism of these observed trends is an issue that requires further study. Although changes to both OHC and OSC are strongly related with the $E - P - R$ field that closely follows the spatial pattern of the latent heat and freshwater fluxes, the role of climatic variability on the OHC and OSC trends is still undetermined. In general, our ability to describe the evolution of such variability is still limited due to the lack of knowledge on the dynamic interaction between oceanic, atmospheric, and hydrological processes (which include the variability of the water budget and its feedback on the precipitation variability, air–sea interactions, rivers discharge, etc.) (Drobinski et al., 2014).

5. Conclusions

The latest hydrographic picture of the Eastern Mediterranean and its sub-regions depicts inter-annual variability that can be generally divided into two periods, 2004–2008 and 2012–2017, that are both characterised by positive trends of temperature and salinity. The first phase, during which many areas are under-sampled, is found to be more variable with abrupt year-to-year changes whilst, the second presents gradual positive trends and more homogeneity across the different regions. Especially after 2013, the yearly average temperature and salinity positive trends at the intermediate, and deep layers, leads to a warming and salinization that exceeds 0.06 °C and 0.02 psu respectively. During the years 2008–2012 a transition period with intense variability separates the two phases. In the beginning of this period (2007–2008), an abrupt increase of both temperature and salinity in the Levantine and Ionian basins is recorded which is followed by an abrupt decrease (2011) in both salt and heat content across the wider area. The most important remarks and results from this study and can be summarised as follows:

1 In the upper layers, positive salinity trends are recorded due to the weakening of the AW signal after 2006 with the only exception of the year 2011. This general status is intensified by the extended presence of LSW in the eastern part of the EMED which spreads, especially after 2010, towards the western and northern parts. After 2012, surface salinity is considerably higher in all sub-basins, except for of 2014 in the Ionian - Adriatic areas.
2 The depicted variability of the surface salinity - density field determines deep homogenisation and DWF events in each sub-region whilst, being strongly correlated with the basin's upper layers circulation, and more specifically with the alternations of the NIG mode.
3 DWF events are identified in the central and eastern Levantine mainly during the first period (2007–2010), and after 2016, resulting in increased LIW production. In the rest of the sub-basins, areas of deep homogenisation are also traced during 2012–2017. In particular, the Adriatic has been a major source of deep-water production for the last 5 years, whilst similar, but lower activity was recorded in the Aegean and Ionian during the same period.
4 At the intermediate depths, the LIW signal dominates. Especially in the Levantine, reaching its peak during 2008–2010. In the same layers, the identification of intense temporal variability in the salinity-density field highlights convection and advection areas.
5 The 1000–1200 m zones of the Aegean and Adriatic are not ventilated by DWF activity, and are mainly occupied by older water masses produced in EMT and pre-EMT periods. Throughout the area of study, the deep-water masses below the 1200 m horizon depict a well-distinguished east to west gradient of both temperature and salinity. The deep ventilation of the 1200–1500 m layer zone presents a slow warming and salinization process especially in the eastern Levantine after 2011 and in the south Ionian after 2013.
6. The OHC in the 100–1000 m depth zone presents a general positive trend with estimated average energy transfer rates, significantly larger than what is reported for the global ocean.
7. Similarly, the OSC in the 10–1000 m zone presents a positive trend that reflects a general increase of salt per profile. This trend is accentuated especially after 2011. A strong west–east positive salinity gradient is observed within the first few hundred meters of the water column.
8. Both heat and salt content are uniformly distributed in the different depth zones within the first 1000 m of the water column after 2014.

During the previous period, differential heat and salt transfer is observed amongst distinct depth zones reflecting intermediate water formation. The heat and salt instabilities eventually resulted in deeper mixing, and advection processes.

Within this study, an updated hydrographic picture of the Eastern Mediterranean area is presented, although there are still open questions regarding our understanding of the processes and dynamics of the Eastern Mediterranean hydrological cycles, and their response to climatic signals. The available profile data from Argo floats has been proved a valuable source of information regarding the Eastern Mediterranean hydrography. The previously discussed constraints of the Argo profile dataset and its ability to sample hydrological contrasts, underlines the need for further combined analysis using additional combo datasets such as ISHII, EN4, or even ocean-model data. However, although the uncertainty induced due to the sparse and inhomogeneous sampling is high, especially during the first years of the study period, the increased data coverage after 2012 can lead to conclusive results regarding the spatio-temporal variability and trends of the water-column physical properties. This highlights the necessity of sufficient float deployments in the Mediterranean Sea that will lead to the increased coverage of such high variable transitional areas.

Declaration of competing interest

The authors declare that they have no known competing financial interests or personal relationships that could have appeared to influence the work reported in this paper.

Acknowledgements

These data were collected and made freely available by the International Argo Program and the national programs that contribute to it. (http://www.argo.ucsd.edu, http://argo.jcommops.org). The Argo Program is part of the Global Ocean Observing System. http://doi.org/10.17882/42182.

The data were downloaded by the Coriolis Global Data Assembly Centre (http://www.coriolis.eu.org).

The authors would like to thank Dr. Laura Bray (lbray@hcmr.gr) and Dr. Nathalie Yonow (N.Yonow@Swansea.ac.uk) for the provision of language assistance.

Appendix A. Supplementary data

Supplementary data to this article can be found online at https://doi.org/10.1016/j.dsr2.2019.104712.

Funding sources

This research did not receive any specific grant from funding agencies in the public, commercial, or not-for-profit sectors.

References

Balmaseda, M.A., Trenberth, K.E., Källén, E., 2013. Distinctive climate signals in reanalysis of global ocean heat content. Geophys. Res. Lett. 40, 1754–1759. https://doi.org/10.1002/grl.50382.

Bergamasco, A., Malanotte-Rizzoli, P., 2010. The circulation of the Mediterranean Sea: a historical review of experimental investigations. Adv. Oceanogr. Limnol. 1, 11–28. https://doi.org/10.1080/19475721.2010.491656.

Béthoux, J.-P., Gentili, B., Tailliez, D., 1998. Warming and freshwater budget change in the Mediterranean since the 1940s, their possible relation to the greenhouse effect. Geophys. Res. Lett. 25, 1023–1026. https://doi.org/10.1029/98GL00724.

Borzelli, G.L.E., Gačić, M., Cardin, V., Civitarese, G., 2009. Eastern mediterranean transient and reversal of the Ionian Sea circulation. Geophys. Res. Lett. 36, L15108. https://doi.org/10.1029/2009GL039261.

Cardin, V., Civitarese, G., Hainbucher, D., Bensi, M., Rubino, A., 2015. Thermohaline properties in the Eastern Mediterranean in the last three decades: is the basin returning to the pre-EMT situation? Ocean Sci. 11, 53–66. https://doi.org/10.5194/os-11-53-2015.

Cheng, L., Trenberth, K.E., Palmer, M.D., Zhu, J., Abraham, J.P., 2016. Observed and simulated full-depth ocean heat-content changes for 1970–2005. Ocean Sci. 12, 925–935. https://doi.org/10.5194/os-12-925-2016.

de Boyer Montégut, C., Madec, G., Fischer, A.S., Lazar, A., Iudicone, D., 2004. Mixed layer depth over the global ocean: an examination of profile data and a profile-based climatology. J. Geophys. Res. Oceans 109, C12003. https://doi.org/10.1029/2004JC002378.

D'Ortenzio, F., Iudicone, D., Montegut, C. de B., Testor, P., Antoine, D., Marullo, S., Santoleri, R., Madec, G., 2005. Seasonal variability of the mixed layer depth in the Mediterranean Sea as derived from in situ profiles. Geophys. Res. Lett. 32 https://doi.org/10.1029/2005GL022463.

Drobinski, P., Ducrocq, V., Alpert, P., Anagnostou, E., Béranger, K., Borga, M., Braud, I., Chanzy, A., Davolio, S., Delrieu, G., Estournel, C., Boubrahmi, N.F., Font, J., Grubišić, V., Gualdi, S., Homar, V., Ivančan-Picek, B., Kottmeier, C., Kotroni, V., Lagouvardos, K., Lionello, P., Llasat, M.C., Ludwig, W., Lutoff, C., Mariotti, A., Richard, E., Romero, R., Rotunno, R., Roussot, O., Ruin, I., Somot, S., Taupier-Letage, I., Tintore, J., Uijlenhoet, R., Wernli, H., Drobinski, P., Ducrocq, V., Alpert, P., Anagnostou, E., Béranger, K., Borga, M., Braud, I., Chanzy, A., Davolio, S., Delrieu, G., Estournel, C., Boubrahmi, N.F., Font, J., Grubišić, V., Gualdi, S., Homar, V., Ivančan-Picek, B., Kottmeier, C., Kotroni, V., Lagouvardos, K., Lionello, P., Llasat, M.C., Ludwig, W., Lutoff, C., Mariotti, A., Richard, E., Romero, R., Rotunno, R., Roussot, O., Ruin, I., Somot, S., Taupier-Letage, I., Tintore, J., Uijlenhoet, R., Wernli, H., 2014. HyMeX: a 10-year multidisciplinary program on the mediterranean water cycle [WWW Document]. Httpsdoiorg101175BAMS–12-002421. https://doi.org/10.1175/BAMS-D-12-00242.1.

Gačić, M., Borzelli, G.L.E., Civitarese, G., Cardin, V., Yari, S., 2010. Can internal processes sustain reversals of the ocean upper circulation? The Ionian Sea example. Geophys. Res. Lett. 37, L09608. https://doi.org/10.1029/2010GL043216.

Gačić, M., Civitarese, G., Kovačević, V., Ursella, L., Bensi, M., Menna, M., Cardin, V., Poulain, P.-M., Cosoli, S., Notarstefano, G., Pizzi, C., 2014. Extreme winter 2012 in the Adriatic: an example of climatic effect on the BiOS rhythm. Ocean Sci. 10, 513–522. https://doi.org/10.5194/os-10-513-2014.

Gaillard, F., Reynaud, T., Thierry, V., Kolodziejczyk, N., von Schuckmann, K., 2015. In situ–based reanalysis of the global ocean temperature and salinity with ISAS: variability of the heat content and steric height. J. Clim. 29, 1305–1323. https://doi.org/10.1175/JCLI-D-15-0028.1.

Guibout, P., 1987. Atlas Hydrographique de la Mediterranée.

Jordà, G., Von Schuckmann, K., Josey, S.A., Caniaux, G., García-Lafuente, J., Sammartino, S., Özsoy, E., Polcher, J., Notarstefano, G., Poulain, P.-M., Adloff, F., Salat, J., Naranjo, C., Schroeder, K., Chiggiato, J., Sannino, G., Macías, D., 2017. The Mediterranean Sea heat and mass budgets: estimates, uncertainties and perspectives. Prog. Oceanogr. 156, 174–208. https://doi.org/10.1016/j.pocean.2017.07.001.

Josey, S.A., 2003. Changes in the heat and freshwater forcing of the eastern Mediterranean and their influence on deep water formation. J. Geophys. Res. Oceans 108. https://doi.org/10.1029/2003JC001778.

Kassis, D., Korres, G., Konstantinidou, A., Perivoliotis, L., 2017. Comparison of high resolution hydrodynamic model outputs with in-situ Argo profiles in the Ionian Sea. Mediterr. Mar. Sci. 18, 22–37. https://doi.org/10.12681/mms.1753.

Kassis, D., Korres, G., Petihakis, G., Perivoliotis, L., 2015. Hydrodynamic variability of the Cretan Sea derived from Argo float profiles and multi-parametric buoy measurements during 2010–2012. Ocean Dyn. 65, 1585–1601. https://doi.org/10.1007/s10236-015-0892-0.

Kassis, D., Krasakopoulou, E., Korres, G., Petihakis, G., Triantafyllou, G.S., 2016. Hydrodynamic features of the South Aegean Sea as derived from Argo T/S and dissolved oxygen profiles in the area. Ocean Dyn. 1–18 https://doi.org/10.1007/s10236-016-0987-2.

Klein, B., Roether, W., Manca, B.B., Bregant, D., Beitzel, V., Kovacevic, V., Luchetta, A., 1999. The large deep water transient in the Eastern Mediterranean. Deep-Sea Res. Part A Oceanogr. Res. Pap. 46, 371–414. https://doi.org/10.1016/S0967-0637(98)00075-2.

Kress, N., Gertman, I., Herut, B., 2014. Temporal evolution of physical and chemical characteristics of the water column in the Easternmost Levantine basin (Eastern Mediterranean Sea) from 2002 to 2010. J. Mar. Syst. 135, 6–13. https://doi.org/10.1016/j.jmarsys.2013.11.016. Assessing and modelling ecosystem changes in the Mediterranean and the Black Sea pelagic ecosystem - SESAME.

Krokos, G., Aarts, G., Velaoras, D., Korres, G., Perivoliotis, L., Theocharis, A., 2014. On the continuous functioning of an internal mechanism that drives the Eastern Mediterranean thermohaline circulation: the recent activation of the Aegean Sea as a dense water source area. J. Mar. Syst. 129, 484–489. https://doi.org/10.1016/j.jmarsys.2013.10.002.

Lascaratos, A., Williams, R.G., Tragou, E., 1993. A mixed-layer study of the formation of Levantine intermediate water. J. Geophys. Res. Oceans 98, 14739–14749. https://doi.org/10.1029/93JC00912.

Lascaratos, A., Roether, W., Nittis, K., Klein, B., 1999. Recent changes in deep water formation and spreading in the eastern Mediterranean Sea: a review. Prog. Oceanogr. 44, 5–36. https://doi.org/10.1016/S0079-6611(99)00019-1.

Levitus, S., Antonov, J.I., Boyer, T.P., Baranova, O.K., Garcia, H.E., Locarnini, R.A., Mishonov, A.V., Reagan, J.R., Seidov, D., Yarosh, E.S., Zweng, M.M., 2012. World Ocean Heat Content and Thermosteric Sea Level Change (0–2000 M). Geophys. Res. Lett. 39 https://doi.org/10.1029/2012GL051106, 1955–2010.

Malanotte-Rizzoli, P., Hecht, A., 1988. Large-scale properties of the eastern Mediterranean: a review. Oceanol. Acta 11, 323–335.

Malanotte-Rizzoli, P., Manca, B.B., d'Alcala, M.R., Theocharis, A., Brenner, S., Budillon, G., Ozsoy, E., 1999. The Eastern Mediterranean in the 80s and in the 90s: the big transition in the intermediate and deep circulations. Dyn. Atmos. Oceans 29, 365–395. https://doi.org/10.1016/S0377-0265(99)00011-1.

Malanotte-Rizzoli, P., Robinson, A.R., 1988. POEM: physical Oceanography of the eastern mediterranean. Eos Trans. Am. Geophys. Union 69, 194–203. https://doi.org/10.1029/88EO00125.

Mantziafou, A., Lascaratos, A., 2008. Deep-Water Formation in the Adriatic Sea: interannual simulations for the years 1979–1999. Deep-Sea Res. Part A Oceanogr. Res. Pap. 55, 1403–1427. https://doi.org/10.1016/j.dsr.2008.06.005.

Mariotti, A., Struglia, M.V., Zeng, N., Lau, K.-M., 2002. The hydrological cycle in the mediterranean region and implications for the water budget of the Mediterranean sea. J. Clim. 15, 1674–1690. https://doi.org/10.1175/1520-0442(2002)015<1674:THCITM>2.0.CO;2.

Mariotti, A., 2010. Recent changes in the mediterranean water cycle: a pathway toward long-term regional hydroclimatic change? J. Clim. 23, 1513–1525. https://doi.org/10.1175/2009JCLI3251.1.

Marshall, J., Schott, F., 1999. Open-ocean convection: observations, theory, and models. Rev. Geophys. 37, 1–64. https://doi.org/10.1029/98RG02739.

Millot, C., 1987. Circulation in the western Mediterranean sea. Oceanol. Acta 10, 143–149.

Nykjaer, L., 2009. Mediterranean Sea surface warming 1985–2006. Clim. Res. 39, 11–17. https://doi.org/10.3354/cr00794.

Ovchinnikov, I.M., P, E., 1976. Hydrology of the Mediterranean sea. Gidrometeoizdat LeningradUSSR 1976, 375.

Ozer, T., Gertman, I., Kress, N., Silverman, J., Herut, B., 2017. Interannual thermohaline (1979–2014) and nutrient (2002–2014) dynamics in the Levantine surface and intermediate water masses, SE Mediterranean Sea. Glob. Planet. Change 151, 60–67. https://doi.org/10.1016/j.gloplacha.2016.04.001. Climate Variability and Change in the Mediterranean Region.

Özsoy, E., Hecht, A., Ünlüata, Ü., 1989. Circulation and hydrography of the Levantine Basin. Results of POEM coordinated experiments 1985–1986. Prog. Oceanogr. 22, 125–170. https://doi.org/10.1016/0079-6611(89)90004-9.

Poulain, P., Barbanti, R., Font, J., Cruzado, A., Millot, C., Gertman, I., Griffa, A., Molcard, A., Rupolo, V., Le Bras, S., De La Villeon, L., 2007. MedArgo: a drifting profiler program in the Mediterranean Sea. Ocean Sci. 3, 379–395.

Riser, S.C., Freeland, H.J., Roemmich, D., Wijffels, S., Troisi, A., Belbéoch, M., Gilbert, D., Xu, J., Pouliquen, S., Thresher, A., Le Traon, P.-Y., Maze, G., Klein, B., Ravichandran, M., Grant, F., Poulain, P.-M., Suga, T., Lim, B., Sterl, A., Sutton, P., Mork, K.-A., Vélez-Belchí, P.J., Ansorge, I., King, B., Turton, J., Baringer, M., Jayne, S.R., 2016. Fifteen years of ocean observations with the global Argo array. Nat. Clim. Chang. 6, 145–153. https://doi.org/10.1038/nclimate2872.

Robinson, A.R., Malanotte-Rizzoli, P., Hecht, A., Michelato, A., Roether, W., Theocharis, A., Ünlüata, Ü., Pinardi, N., Artegiani, A., Bergamasco, A., Bishop, J., Brenner, S., Christianidis, S., Gacic, M., Georgopoulos, D., Golnaraghi, M., Hausmann, M., Junghaus, H.-G., Lascaratos, A., Latif, M.A., Leslie, W.G., Lozano, C. J., Oguz, T., Özsoy, E., Papageorgiou, E., Paschini, E., Rozentroub, Z., Sansone, E., Scarazzato, P., Schlitzer, R., Spezie, G.-C., Tziperman, E., Zodiatis, G., Athanassiadou, L., Gerges, M., Osman, M., 1992. General circulation of the eastern mediterranean. Earth Sci. Rev. 32, 285–309. https://doi.org/10.1016/0012-8252(92)90002-B.

Roether, W., Klein, B., Manca, B.B., Theocharis, A., Kioroglou, S., 2007. Transient Eastern Mediterranean deep waters in response to the massive dense-water output of the Aegean Sea in the 1990s. Prog. Oceanogr. 74, 540–571. https://doi.org/10.1016/j.pocean.2007.03.001.

Roether, W., Manca, B.B., Klein, B., Bregant, D., Georgopoulos, D., Beitzel, V., Kovačević, V., Luchetta, A., 1996. Recent changes in eastern mediterranean deep waters. Science 271, 333–335. https://doi.org/10.1126/science.271.5247.333.

Roether, W., Schlitzer, R., 1991. The Mediterranean Sea Eastern Mediterranean deep water renewal on the basis of chlorofluoromethane and tritium data. Dyn. Atmos. Oceans 15, 333–354. https://doi.org/10.1016/0377-0265(91)90025-B.

Schroeder, K., Chiggiato, J., Josey, S.A., Borghini, M., Aracri, S., Sparnocchia, S., 2017. Rapid response to climate change in a marginal sea. Sci. Rep. 7, 4065. https://doi.org/10.1038/s41598-017-04455-5.

Schroeder, K., Millot, C., Bengara, L., Ben Ismail, S., Bensi, M., Borghini, M., Budillon, G., Cardin, V., Coppola, L., Curtil, C., Drago, A., El Moumni, B., Font, J., Fuda, J.L., García-Lafuente, J., Gasparini, G.P., Kontoyiannis, H., Lefevre, D., Puig, P., Raimbault, P., Rougier, G., Salat, J., Sammari, C., Sánchez Garrido, J.C., Sanchez-Roman, A., Sparnocchia, S., Tamburini, C., Taupier-Letage, I., Theocharis, A., Vargas-Yáñez, M., Vetrano, A., 2013. Long-term monitoring programme of the hydrological variability in the Mediterranean Sea: a first overview of the HYDROCHANGES network. Ocean Sci. 9, 301–324. https://doi.org/10.5194/os-9-301-2013.

Skliris, N., 2014. Past, present and future patterns of the thermohaline circulation and characteristic water masses of the Mediterranean sea. The Mediterranean Sea. Springer, Dordrecht, pp. 29–48. https://doi.org/10.1007/978-94-007-6704-1_3.

Skliris, N., Sofianos, S., Lascaratos, A., 2007. Hydrological changes in the Mediterranean Sea in relation to changes in the freshwater budget: a numerical modelling study. J. Mar. Syst. 65, 400–416. https://doi.org/10.1016/j.jmarsys.2006.01.015. Marine Environmental Monitoring and Prediction.

Theocharis, A., Georgopoulos, D., Lascaratos, A., Nittis, K., 1993. Water masses and circulation in the central region of the eastern mediterranean: eastern ionian, south Aegean and northwest levantine, 1986–1987. Deep Sea Res. Part II Top. Stud. Oceanogr. 40, 1121–1142. https://doi.org/10.1016/0967-0645(93)90064-T.

Theocharis, A., Krokos, G., Velaoras, D., Korres, G., 2014. An internal mechanism driving the alternation of the eastern mediterranean dense/deep water sources. In: Borzelli, G.L.E., Gačić, M., Lionello, P., Paolalanotte-Rizzoli (Eds.), The Mediterranean Sea. John Wiley & Sons, Inc., pp. 113–137

Theocharis, A., Nittis, K., Kontoyiannis, H., Papageorgiou, E., Balopoulos, E., 1999. Climatic changes in the Aegean Sea influence the eastern Mediterranean thermohaline circulation (1986–1997). Geophys. Res. Lett. 26, 1617–1620. https://doi.org/10.1029/1999GL900320.

Tsimplis, M.N., Josey, S.A., 2001. Forcing of the Mediterranean sea by atmospheric oscillations over the north Atlantic. Geophys. Res. Lett. 28, 803–806.

Velaoras, D., Kassis, D., Perivoliotis, L., Pagonis, P., Hondronasios, A., Nittis, K., 2013. Temperature and salinity variability in the Greek Seas based on POSEIDON stations time series: preliminary results. Mediterr. Mar. Sci. 14, 5–18.

Velaoras, D., Krokos, G., Nittis, K., Theocharis, A., 2014. Dense intermediate water outflow from the Cretan Sea: a salinity driven, recurrent phenomenon, connected to thermohaline circulation changes. J. Geophys. Res. Oceans 119, 4797–4820.

Velaoras, D., Krokos, G., Theocharis, A., 2015. Recurrent intrusions of transitional waters of Eastern Mediterranean origin in the Cretan Sea as a tracer of Aegean Sea dense water formation events. Prog. Oceanogr. 135, 113–124.

Velaoras, D., Papadopoulos, V.P., Kontoyiannis, H., Papageorgiou, D.K., Pavlidou, A., 2017. The response of the Aegean Sea (eastern mediterranean) to the extreme 2016–2017 winter. Geophys. Res. Lett. 44, 9416–9423.

Von Schuckmann, K., Gaillard, F., Le Traon, P.-Y., 2009. Global hydrographic variability patterns during 2003–2008. J. Geophys. Res. Oceans 114. https://doi.org/10.1029/2008JC005237.

Von Schuckmann, K., Sallée, J.-B., Chambers, D., Le Traon, P.-Y., Cabanes, C., Gaillard, F., Speich, S., Hamon, M., 2014. Consistency of the current global ocean observing systems from an Argo perspective. Ocean Sci. 10, 547–557. https://doi.org/10.5194/os-10-547-2014.

Wong, A.P.S., Johnson, G.C., Owens, W.B., 2003. Delayed-mode calibration of autonomous CTD profiling float salinity data by θ–S climatology. J. Atmos. Ocean. Technol. 20, 308–318. https://doi.org/10.1175/1520-0426(2003)020<0308:DMCOAC>2.0.CO;2.

Wu, P., Haines, K., 1996. Modeling the dispersal of Levantine Intermediate Water and its role in Mediterranean deep water formation. J. Geophys. Res. Oceans 101, 6591–6607. https://doi.org/10.1029/95JC03555.

Zervakis, V., Georgopoulos, D., 2002. Hydrology and circulation in the north Aegean (eastern mediterranean) throughout 1997 and 1998. Mediterr. Mar. Sci. 3, 5–19.